DETECTION OF INDUCTION MOTOR FAULTS USING VIBRATION, CURRENT AND ACOUSTIC DATA

Murat BAŞARAN

Ph.D. Dissertation

Graduate School of Science
Electrical and Electronics
Engineering Program

April-2016

JÜRİ VE ENSTİTÜ ONAYI

Murat BAŞARAN'ın **"Titreşim, Akım ve Ses Verileri Kullanarak Asenkron Motor Arızalarının Belirlenmesi"** başlıklı **Elektrik-Elektronik Mühendisliği** Anabilim Dalındaki, Doktora Tezi 09.03.2016 tarihinde, aşağıdaki jüri tarafından Anadolu Üniversitesi Lisansüstü Eğitim-Öğretim ve Sınav Yönetmeliğinin ilgili maddeleri uyarınca değerlendirilerek kabul edilmiştir.

		Adı Soyadı	İmza
Üye (Tez Danışmanı) :		**Prof. Dr. DOĞAN GÖKHAN ECE**	**……..**
Üye	**:**	**Prof. Dr. ÖMER NEZİH GEREK**	**……..**
Üye	**:**	**Prof. Dr. MEHMET KURBAN**	**……..**
Üye	**:**	**Doç. Dr. SERKAN GÜNAL**	**……..**
Üye	**:**	**Yrd. Doç. Dr. MEHMET KOÇ**	**……..**

Anadolu Üniversitesi Fen Bilimleri Enstitüsü Yönetim Kurulu'nun …….. tarih ve …….. sayılı kararıyla onaylanmıştır.

Enstitü Müdürü

ABSTRACT

Ph.D. Dissertation

DETECTION OF INDUCTION MOTOR FAULTS USING VIBRATION, CURRENT AND ACOUSTIC DATA

Murat BAŞARAN

Anadolu University
Graduate School of Sciences
Electrical and Electronics Engineering Program

Supervisor: Prof. Dr. Doğan Gökhan ECE

2016, 71 pages

Early diagnostics of incipient faults in induction motors is an important aspect of preventive maintenance strategies. In this thesis, frequently encountered induction motor fault types are detected and classified using stator current, vibration and acoustic data. Current, vibration and acoustic that data are acquired from the experiments realized under different loading conditions of induction motors on which different fault types created synthetically are used for feature extraction by means of different signal processing techniques including Wavelet Packet Decomposition, 2D Wavelet Transform and Local Binary Patterns. Conversion of one-dimensional data signals into two-dimensional grayscale images whose sizes are arranged due to their autocorrelation value provide the opportunity of utilization of texture based methods for feature extraction. Novel feature vectors are proposed for fault classification and their performances are tested with Neural Network and Bayesian based classifiers. Besides, a remarkable benchmark database is constructed consisting of stator current, vibration and acoustic data acquired under many operating conditions. This database is expected to be used as medium for future works of fault diagnosis related to preventive maintenance strategies of the induction motors.

Keywords: Induction motors, Fault detection, Wavelet Packet Decomposition, 2D Wavelet Transform, Local Binary Patterns, Preventive maintenance

ÖZET

Doktora Tezi

TİTREŞİM, AKIM VE SES VERİLERİ KULLANARAK ASENKRON MOTOR ARIZALARININ BELİRLENMESİ

Murat BAŞARAN

Anadolu Üniversitesi
Fen Bilimleri Enstitüsü
Elektrik-Elektronik Mühendisliği Anabilim Dalı

Danışman: Prof. Dr. Doğan Gökhan ECE

2016, 71 sayfa

Asenkron motorların başlangıç seviyesindeki arızalarının önceden tespit edilmesi koruyucu bakım stratejilerinin önemli bir unsurudur. Bu tez çalışmasında stator akımı, titreşim ve ses verileri kullanılarak asenkron motorlarda sıklıkla karşılaşılan arıza tipleri tespit edilmiş ve sınıflandırılmıştır. Üzerlerinde farklı arıza tiplerinin kasıtlı olarak oluşturulduğu asenkron motorların farklı yükleme koşulları altında çalıştırması deneylerinden elde edilen akım, titreşim ve ses verilerinden Dalgacık Paket Ayrıştırması, İki-boyutlu Dalgacık Dönüşümü, Yerel İkili Örüntüler gibi çeşitli sinyal işleme yöntemleri ile sınıflandırmada kullanılacak öznitelikler çıkarılmıştır. Tek boyutlu veri sinyallerinin otokorelasyon değerlerine göre boyutları ayarlanmış iki boyutlu gri tonlu imgelere dönüştürülmesi öznitelik çıkarımında doku analizi tabanlı yöntemlerin kullanılmasına olanak tanımıştır. Arıza sınıflandırma için yenilikçi öznitelik vektörleri önerilmiş ve sınıflandırma performansları Yapay Sinir Ağları ve Bayes tabanlı sınıflandırıcılar ile test edilmiştir. Farklı arıza tiplerine sahip motorlardan farklı yükleme koşulları altında elde edilmiş, stator akımı, titreşim ve ses verilerini içeren bir veri tabanı oluşmuş olup bu veri tabanının gelecekte yapılacak koruyucu bakım çalışmaları için değerli bir kaynak olması beklenmektedir.

Anahtar Kelimeler: Asenkron motorlar, Arıza tespiti, Dalgacık Paket Ayrıştırması, İki-boyutlu Dalgacık Dönüşümü, Yerel İkili Örüntüler, Koruyucu bakım

ACKNOWLEDGEMENTS

First, I would like to thank my supervisor, Prof. Dr. Doğan Gökhan ECE for his continuous support and guidance throughout my thesis work. I would like to thank Prof. Dr. Ömer Nezih GEREK for his valuable contributions and remarkable comments to my thesis. Also I would like to thank Assoc. Prof. Dr. Serkan GÜNAL for his support and constructive comments during my thesis work.

Then I would like to thank Prof. Dr. Mehmet KURBAN and Assist. Prof. Dr. Mehmet KOÇ for their support and valuable comments to my thesis. Also I am thankful to Assist. Prof. Dr. Emin GERMEN and Assist. Prof. Dr. Mehmet FİDAN for their active support and contributions to my thesis work.

Finally, I would like to thank my wife, brother, and parents for their confidence and moral support.

Murat BAŞARAN

April, 2016

TABLE OF CONTENTS

LIST OF FIGURES

LIST OF TABLES

LIST OF ACRONYMS

AC	: Alternating Current
ASD	: Adjustable Speed Drive
AM	: Amplitude Modulation
ANN	: Artificial Neural Network
CVA	: Common vector approach
DC	: Direct Current
DWT	: Discrete Wavelet Transformation
EMF	: Electromotive Force
FFT	: Fast Fourier Transform
HMM	: Hidden Markov Model
HP	: High-pass
IEPE	: Integrated Electronic Piezoelectric
LBP	: Local Binary Pattern
LDA	: Linear Discriminant Analysis
LDC	: Linear Discriminant Classifier
LP	: Low-pass
LVQ	: Learning Vector Quantization
MCSA	: Motor Current Signature Analysis
NN	: Neural Network
NFMCSA	: Notch-Filtered Motor Current Signature Analysis
PWM	: Pulse-width Modulation
QDC	: Quadratic Discriminant Classifier
SIFT	: Scale Invariant Feature Transform
SOM	: Self-Organizing Map
SPL	: Sound Pressure Level
SVM	: Support Vector Machine
WPD	: Wavelet Packet Decomposition

1. INTRODUCTION

Electric motors are the most widely used electrical machines in industry. Electric motors consume more than half of the energy demand in developed countries and the consumption is expected to increase in every year depending on the economic and population growth. In 2011, the total number of electric motors operating in industry was around 16.1 billion worldwide. Furthermore, in the last past five years, the number of the operating motors tend to increase with a growth rate of about 50% (Henao et al., 2014). Among all electric motors, the squirrel-cage induction motors, in sizes ranging from fractional horsepower to industry grade, are the most commonly used electric motors in industrial installations. Due to their simple construction, cost effectiveness and easy maintenance, the squirrel cage induction motors are the most preferable electrical motors in the industry. The global competition on the production industry enforce the companies to continue their industrial operations more reliably with high efficiency. In order not to interrupt the industrial processes caused by unexpected failures of induction motors, preventive maintenance strategies are essential. Early diagnostics of incipient faults in induction motors are important to ensure safe operation and help to recognize and fix the problems with low cost and time.

An induction motor can be simply defined as an asynchronous machine which converts energy from the electrical to mechanical form by means of electromagnetic induction. An induction motor consists of many parts as shown in Figure 1.1. The essential parts of a squirrel-cage induction motor are a wound stator and a squirrel-cage rotor. The rotor of the motor comprises a squirrel-cage rotor which consists of conducting bars embedded in slots that are short circuited at both ends by conducting end rings, a rotor shaft and lamination stacks. The rotor bars are enveloped by a laminated iron core that concentrates the magnetic flux from the stator windings and also the iron core mechanically supports the shaft. Also there is a small space between the stator and the rotor which is named as air-gap. The bearings are located on the both sides of the shaft, which are the mechanically rotating parts of the motors having a set of spherical or cylindrical rolling elements inside two circular rings that allow rotor shaft to spin freely inside the motor. The

stator of the motor comprises the frame, lamination core and the stator windings. The frame mechanically supports the stator and the bearings located at the ends of the rotor shaft. The stator windings are composed of three equally distributed coils along the stator lamination core. These windings are electrically shifted by 120°. These electrically shifted windings can be supplied either directly by 3 phase AC network or by the output of a frequency inverter. In both cases, only stator coils are connected with the power line. When a current *i* passes through stator coils, it induces a magnetic field H, which is proportional to the current (Chapman, 2005). When three phase voltage is applied, three stator phase currents generate three magnetic fields. Since the currents are phase shifted by 120°, these magnetic fields are also shifted by 120°. The energy for the rotor is delivered by means of induction by the synchronous rotation of the stator magnetic field and this phenomenon gives the name "induction motor" for these kind of electrical machines (Fitzgerald et al., 1990). Since opposite poles attract each other, the rotor follows the rotating magnetic field of the stator resulting in a rotation slightly slower than the rotating magnetic field of the stator and the difference in rotational speed is called the slip speed.

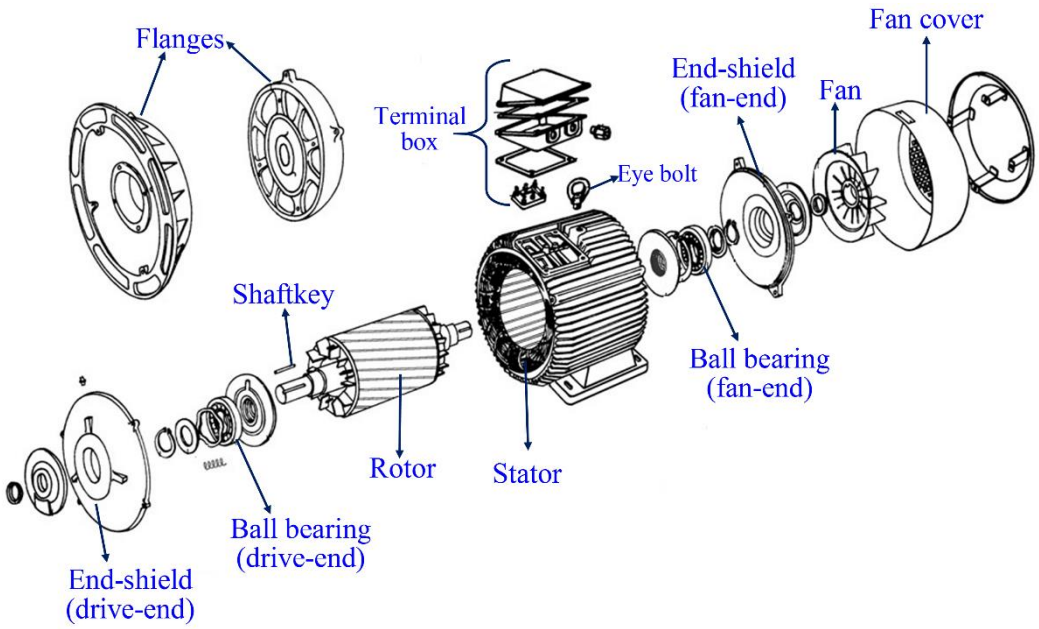

Figure 1.1. Parts of a squirrel-cage induction motor

1.1. Literature Overview

Induction motors are being used increasingly in many industrial and commercial applications such as cranes, lifts, conveyors, pumps, fans, heating and ventilation systems and various type of manufacturing systems. Incipient type of faults such as cracked or broken rotor bars or end-rings, opening or shorting of one or more of a stator phase winding, minor bearing damages, static or dynamic air-gap irregularities, and misalignments which do not completely block the rotor, may cause unbalanced air-gap voltages and line currents, increase in noise, decrease in torque, excessive currents and heat during the steady state operation of the motor (Nandi et al., 2005; Acosta et al., 2006). These faults may cause failures resulting downtime in the industrial process and loss of huge investment which can't be compared to the cost of the motor itself or the maintenance costs. Furthermore, unexpected shutdown may result in the interruption of critical services such as medical, military and transportation applications. Downtime is not tolerable in those applications since the continuous process is needed and any interruption may cause huge maintenance costs, even loss of life (Toliyat et al., 2012). Therefore, faults must be detected at their inception by means of preventive maintenance in order to avoid undesirable motor failures.

Induction motors consists of many mechanical and electrical parts such as stator windings, rotor bars, rotor end-rings, ball bearings and terminal box. Each part of induction motors is highly potentially exposed to the risk of unexpected mechanical, chemical and electrical failures due to the harsh industrial working environments. The frequently encountered reasons behind the induction motor failures in industry have been commonly reported as unrated power, voltage and current utilization due to unstable power source, overload or unbalanced load, electrical stresses from fast switching of inverters, grounding problems and residual stresses from manufacturing of the motors. Besides, problems may also originate from harsh industrial working environments such as dust, water leaks, chemical contamination, high temperature and environmental vibration.

In recent years, condition monitoring of induction motors, early fault diagnosis and classification topics become popular among researchers who are

being motivated from the necessity of preventive maintenance strategies in industry. Considerable amount of researches have been focused on the methods for detection of the mechanical and electrical faults in induction motors. More than 300 publications issued until 1999 are listed by Benbouzid in reverse chronological order in a bibliographical manner which can be considered as a great source of information covering these topics (Benbouzid, 1999). After 1999, the amount of research of fault diagnosis methods for detection and classification of different fault types have been increasing so far. Both invasive and noninvasive methods are used to measure motor current, vibration, temperature, speed and torque variations, and acoustic noise for detection of motor abnormalities. However, the most often used method of condition monitoring is the motor current signature analysis (MCSA) since the motor current contains required information for fault detection.

In addition to current spectrum monitoring techniques, mechanical vibration and acoustic monitoring are the commonly used maintenance techniques to prevent motor faults. Vibration monitoring technique requires additional sensors such as accelerometers to be placed on the operating motors. Since permanently placing of accelerometers to every operating motors is not an efficient choice economically, periodical check with portable equipment is more preferable for preventive maintenance. Like vibration monitoring, acoustic monitoring requires additional equipment like microphones, sound amplifiers and recorders. Some motors used in critical applications may not be easily reachable or the working environment may not be suitable to place additional equipment and this drawback makes motor current monitoring more reliable compared to vibration and acoustic monitoring in those situations (Toliyat et al., 2012).

In literature, many time domain methods are proposed which utilize time domain information energy, local extrema, kurtosis and skewness parameters as features which are extracted from the time domain motor stator current signals, sometimes by utilizing different sizes of sliding windows (Günal et al., 2009; Dalvand et al., 2015). Neural Network based classification of induction motor faults using time-domain features are also proposed (Samanta and Al-Balushi, 2003). Besides, an amplitude modulation (AM) detector is proposed to detect incipient type of race defects (Stack et al., 2004).

Well known signal processing tools of Fourier, Wavelet, and Hilbert–Huang transformations are applied to acquired motor current data to extract necessary features for motor fault detection (Benbouzid and Kliman, 2003; Zhang et al., 2003; Douglas et al., 2004; Ayhan et al., 2005; Knight and Bertani, 2005; Yan and Gao, 2006). During steady-state operation, induction motors draw noisy and harmonically rich line current due to their nonlinear characteristics. Spectral methods used for MCSA are employed to extract signature identifiers, namely features to be used for fault classification. Instead of direct use of stator current, applying notch-filter to stator current is another aspect of motor current signature analysis. Notch-filtered motor current signature analysis (NFMCSA) can be considered as another method of induction motor condition monitoring (Günal and Gerek, 2009).

In literature, a generic fault detection approach based on discriminative energy functions is proposed to identify failures where these energy functions display discriminative frequency domain regions related to motor faults (Ilonen et al., 2005).Also the combination of wavelets and support vector machine (SVM) is utilized and MCSA based on induction motor start-up transient current signal is used for fault detection and classification (Widodo et al., 2007). During start-up, since induction motors draw large currents from the supply system, contributions of possible faults to the current spectra is more pronounced and extraction of features due to a fault is easier. Although successful detection and classification results were obtained, the presented method may not be applied without interrupting the process run by the induction motor under investigation (Widodo and Yang, 2008).

Wavelet packet decomposition (WPD) of current signals to solve induction motor fault diagnosis problems is a widely used tool in literature. By proper selection of decomposition level, very narrow frequency resolution can be obtained in order to observe the effects local peaks around the fundamental frequency component on the current spectra of the current signal (Ece and Başaran, 2011).

Vibration measurement is widely used popular technique to detect induction motor faults, especially in faulty bearings problems. However, vibration monitoring can be expensive and cannot always be performed, while electrical quantities such

as stator current are often measured for control and detection purposes of faults. In literature, there are detailed comparative works which states pros and cons of both vibration and current and their theoretical analysis of the physical links between the indications of faults (Immovilli et al., 2010; Trajin et al., 2010). Electric machines produce noise and vibration during operation and these acoustic and vibration signals may indicate that incipient type of fault if exists. Small amplitude of vibration signal may produce relatively high amount of noise. Noise and vibration can be originated by magnetic, mechanical and aero dynamical forces. Vibration data is also utilized in the fault detection and classification problem using genetic algorithms, namely clone selection programming (Gan et al., 2009), and using the combination of SVM with independent component analysis (Widodo et al., 2007). A Hidden Markov Model (HMM) based technique for vibration signals is also developed for bearing fault detection (Ocak and Loparo, 2005). Common vector approach (CVA), which is a well-known subspace-based pattern recognition method that is commonly used in speech and image recognition can also applied to induction motor fault diagnosis with vibration monitoring. A common vector for each class is calculated using the feature vectors in the training set of that class in which the common vector is unique and represents the common properties of that class by means of vibration data processing for bearing fault classification (Gülmezoğlu and Ergin, 2007; Ergin et al., 2012).

In the fault detection process, significant features from vibration signals can be extracted through the scale invariant feature transform (SIFT) algorithm to detect the faulty symptoms with 2D representation of the vibration signals (Chong, 2011). By 2D representation of the signal, texture related features can be extracted. If a priori knowledge of the classes to be recognized is exists, appropriate texture based techniques can be applied for the classifications of the patterns caused by indicators like vibration signals (Tuceryan and Jain, 1993; Arivazhagan and Ganesan, 2003; Avci et al., 2009). Artificial neural network (ANN) based bearing fault classification of bearing faults with vibration spectrum imaging is another example of grayscale to binary image conversion of vibration signal in literature. This work shows the spectral contents of the translation-variant time-segmented vibration signal, transformed into a spectral image (Amar et al., 2015). New approaches for

fault diagnosis of induction motors utilizing two-dimensional texture analysis based on local binary patterns (LBP) is getting popular. Firstly, time domain vibration signals acquired from the operating motors can be converted into two-dimensional grayscale images. Then, discriminating texture features can be extracted from these images employing LBP operator (Shahriar et al., 2013).

Unlike vibration based analysis, there is very limited literature on fault diagnosis of induction motors based on techniques of acoustic analysis. Also some of the works analyze the acoustic data which is recorded in an echo-free silent environment, which seems impractical for the real life applications, especially in industrial processes (Benko et al., 2004). Instead of echo-free silent environment, new approaches are tried with acoustic data collected from noisy environment. By acquiring acoustic data with simultaneous recordings of five microphones, fairly good classification results are obtained in fault classification of motors (Germen et al., 2014). Also the identification of acoustic noise spectra in induction motors by using frequency-domain cross-power spectrum estimation algorithm is a recently developed technique in acoustic based fault classification literature (Akcay and Germen, 2015). For industrial applications, there are few papers related to acoustic analysis that investigates the effects of sound radiation direction in faulty hermetic compressors (Kaya et al., 2008; Germen et al., 2010).

1.2. Thesis Outline

In this thesis, frequently encountered induction motor fault types are explained in Section 2. The magnitude of certain frequency components can be increased by the existing fault mechanism that gives signature of the faults. From the view of the preventive maintenance strategy, the early detection and diagnosis of the fault mechanism is crucial. The motivation of this thesis is to propose novel methods to detect and discriminate incipient type of induction motor faults by using non-invasive methods. From this motivation many different experiments are realized in Power Systems Laboratory of Anadolu University in order to construct a benchmark database consisting of current, vibration and acoustic data. This gives

importance and novelty to the work in literature as it uses three different sources of fault indicators.

In Section 3, experimental setup and data acquisition procedures followed during the experimental works of this thesis are explained. Synthetic creation of faults on test motors and motor experiments under different load conditions both with directly supplied from the AC network and driven by adjustable speed drives are explained in detail. Many different experiments under predetermined speed references and load conditions are realized in order to obtain current, vibration and acoustic data from test motors to classify motor faults.

In Section 4, feature extraction techniques used in thesis from current, vibration and acoustic signals are explained. Wavelet packet decomposition and 2D discrete wavelet transformation is one of the main motivation sources of these techniques. One dimensional data is converted to two dimensional grayscale images to reveal underlying fault mechanism and this method became the motivation under texture based methods like local binary patterns (LBP) applied for feature extraction.

In Section 5, classification Bayesian originated classifiers linear and quadratic discriminant classifiers and Fisher's linear discriminant based classifier are explained. Also Neural Network (NN) based classification algorithm self-organizing maps (SOM) and learning vector quantization (LVQ) techniques are explained which are used in fault classification of current, vibration and sound data obtained from various experiments realized and classification results for different cases are given in Section 6. Classification performances of different type of classifiers and selected filter types are discussed and results are given in tabular format. Also to make a fair comparison, current, vibration and acoustic data performances with same features are discussed to show the convenience of data type for classification. Some scatter plots are also given to show clustering of the selected features on three dimensional space. Concluding remarks for the thesis are given in the last section.

2. FREQUENTLY ENCOUNTERED INDUCTION MOTOR FAULTS

Although squirrel-cage induction motors are rugged and reliable electric machines, they are exposed to many different mechanical and electric stresses which may lead to different types of faults. Frequently encountered induction motor failures can be separated into two main groups according to the reason behind the failure as mechanical and electrical failures.

Electrical faults mainly covers stator and rotor failures such as, opening or shorting of one or more of a stator phase windings, inter-turn short circuits in stator windings and broken rotor bars or end-rings.

Different types of bearing damages and static and dynamic air-gap irregularities resulting from the misalignments between the shaft of the motor and the load can be considered as mechanical faults. The existence of a fault mechanism exhibits itself as unbalanced stator voltages and currents, torque fluctuations, excessive heating of the motor, increase in vibrations, decrease in efficiency and torque. Besides, the magnitude of certain frequency components can be increased by the existing fault mechanism.

Among all types of faults, bearing related motor failures are the most commonly encountered type, which cause roughly almost half of the failure incidents. After bearing faults, electrical faults are the second most encountered fault types which stator winding failures and rotor failures accounts for about 35% and more than 5% share respectively among all failure incidents. The rest of the failure incidents are caused by other types of mechanical faults mainly resulting from misalignments and other axial connection mistakes (Bellini et al., 2008; Tavner, 2008).

2.1. Rotor Bar Faults

Broken or cracked rotor bars and end-rings may cause severe problems in induction motors, which accounts for more than 5% of all industrial motor failures. Although broken rotor bars do not initially cause an induction motor to fail, there can be serious side effects.

The reasons behind the breakage of the rotor bars and end-rings can be several such as the imperfections in the manufacturing of the rotor cage, mechanical stresses caused by vibrating loads, thermal and mechanical stresses caused by direct starting of the motor under overloading conditions which motor is not designed to operate and dynamic stresses arising from shaft torques (Thomson and Fenger, 2001; Nandi et al., 2005). Also the environmental factors like contamination, corrosion and abrasion of the rotor due to chemicals and humidity and the mechanical factors such as loose and weak laminations, wearied parts and the problems related to bearings may cause broken or cracked rotor bar failures.

When the cage winding is symmetrical, there is only a forward rotating field at slip frequency with respect to the rotor. Once a broken rotor bar exists, no current will flow in this rotor bar therefore the field in the rotor around the broken rotor bar will not exist. As a result, the force applied to that side of the rotor would be different from that on the other sides of the rotor and this creates an asymmetric magnetic force that rotates at one times of the rotational speed and modulates at a frequency equal to slip frequency times the number of poles (Finley et al., 1999). Due to the asymmetry, there will be a resultant backward rotating field at slip frequency with respect to the forward rotating rotor. This backward rotating field at slip frequency, induces an electromotive force (EMF) and current in the stator winding at the frequency which is referred to as a twice slip frequency sideband due to broken rotor bars. The analytical expression for the frequencies that are present in the air gap flux is given as:

$$f_{br} = f_0\left(1 \pm 2ns\right) \tag{2.1}$$

where f_0 is line frequency, n is the set of positive integers and s is the per-unit slip of the motor. All of these frequencies should be present in the air gap flux. These are the classical twice slip frequency sidebands due to broken rotor bars. In other words, a broken rotor bar problem actually is an asymmetry of the rotor and it causes torque pulsations, unbalance in line currents and reduce in average torque and induction motors. This asymmetry boosts up the left sideband of the source frequency (Nandi et al., 2005). Broken rotor bar problem can be determined by time

and frequency analysis of the induced voltages. In normal operation, stator winding is supplied with an AC source having f_0 line frequency and rotor bar currents are induced at sf_0 frequencies (Filippetti et al., 1998). When an asymmetry occurs due to the rotor bar problem, stator EMF at $f_0(1 \pm 2s)$ frequencies are induced that causes ripples in speed and torque.

The amplitude of the air gap flux harmonics at the frequencies varies due to the variables that affect the frequency of these sidebands such as rotor design, power rating of the motor, different load conditions and mechanical load characteristics. These factors significantly affect the fault diagnosis process and should be considered for a reliable fault diagnosis system (Kliman et al., 1988).

2.2. Stator Winding Faults

Stator faults in induction motors occur due to normal aging of the insulation, abnormal operating conditions or through a variety of other mishaps. Many of these faults are not immediately catastrophic and they have negligible effect on the operating performance of the motor. However, presence of the faults will ultimately lead to catastrophic failure of motors unless diagnosed (Williamson and Mirzoian, 1985).

The stator is subjected to many types of stresses such as thermal, electrical, mechanical, and environmental which severely affects the stator condition and leading to faults (Tavner and Penman, 1987). Thermal stresses related to the operating temperature of the motors severely affect the insulation such that for every 10^{o}C increase in temperature, the life of insulating material gets halved due to thermal aging. The winding failure will occur if the insulating material loose its physical integrity. The effect of temperature on thermal aging can be minimized either by reducing the operating temperature or by increasing the class of insulation.

Electrical problems such as transient voltage conditions, either turn-to-turn or turn-to-ground, may also cause insulation failures. Short circuits or starting stresses are important electrical problems that may occur in stator windings. The rotor can strike the stator mechanically due to problems like bearing failures, shaft deflection or rotor-to-stator misalignments. If the strike happens only during

startup, then the force of the rotor can cause the stator laminations to puncture the coil insulation. Environmental stresses such as the presence of foreign material such as contamination due to oil, moisture and dirt could cause abnormalities in heat dissipation which cause to increase operating temperature and reduce the life of the insulating material (Siddique et al., 2005). Also improper cooling systems may cause overheating related problems.

In literature, several papers are published on the analysis of air gap and axial flux signals to detect shorted turns (Penman et al., 1994). The components in the air gap flux waveform that are a function of shorted tums can be given by the equation:

$$f_{sw} = f_0\left[k \pm \frac{n}{p}(1-s)\right] \tag{2.2}$$

where f_0 is the line frequency, k is set of positive odd integers, n is set of positive integers, p is the number of pole pairs in the motor and s is the per-unit slip of the motor (Thomson, 2001). The diagnosis of shorted turns via MCSA is based on detecting the frequency components given by equation in that these rotating flux waves can induce corresponding current components in the stator winding.

2.3. Bearing Faults

Bearing are the mechanical rotating parts of the motors having a set of spherical or cylindrical rolling elements inside two circular rings. The outer ring is embedded into the motor frame and named as outer race. The inside ring is called as inner race and it clutches the shaft of the motor. Most of the induction motors run under non-ideal conditions in industrial applications and bearing of the motors are subject to many different corrosive factors. These non-ideal operating conditions may lead incipient type of bearing faults which tend to deteriorate and propagate on to the races and the rolling elements of the bearings.

In the case of a bearing defect, abnormal mechanical noise, excessive heating, and some amount of over-current due to the slight blocking effect of the defective bearing to the rotating motor shaft will occur. The reasons behind bearing

deficiencies are various. Mechanical factors like improper or loose connection of the motor shaft and unbalanced motor loads cause excessive vibrations which leads to deteriorations inside the bearings. Also aging is another important factor. Long time utilization of the motor, even under normal operating conditions, wears the bearings and cause excessive vibrations and noise. Some working environments can cause contamination due to the moisture and abrasion of bearing elements occur. These abrasions may lead to cracks unless the necessary maintenance is made. Improper and insufficient lubrication of the bearings are other aspects which increase the abrasion of the material by excessive friction and heat. It is also possible to encounter bearing faults as rotor asymmetry faults, which usually referred as eccentricity faults.

Basically, bearing related deficiencies can be categorized as outer bearing race defect, inner bearing race defect, ball defect and cage defect. The vibration frequencies to detect these faults can be given as formulas as a function of rotational frequency and the bearing geometry. The four characteristic vibration frequencies, f_v in Hertz (Hz) related to each type of faults can be given respectively as follows:

$$f_{or} = \left(N_b / 2\right) f_r \left[1 - d_b \cos\left(\beta\right) / d_p\right] \tag{2.3}$$

$$f_{ir} = \left(N_b / 2\right) f_r \left[1 + d_b \cos\left(\beta\right) / d_p\right] \tag{2.4}$$

$$f_{bd} = d_p f_r / 2 d_b \left[1 - (d_b \cos\left(\beta\right) / d_p)^2\right] \tag{2.5}$$

$$f_{cd} = \left(f_r / 2\right)\left[1 - d_b \cos\left(\beta\right) / d_p\right] \tag{2.6}$$

where f_r is the rotational speed, N_b is the number of balls between the races, β is the contact angle of the ball with the races, d_b and d_p are the ball diameter and the pitch diameter respectively, which can be seen in Figure 2.1. These characteristic vibration frequencies reflect themselves in the current spectrum as:

$$f_{bf} = \left| f_0 \pm m \cdot f_v \right| \tag{2.7}$$

where m is the set of positive integers, f_0 is the line frequency and f_v are one of the four characteristic frequencies related to bearing fault type (Schoen et al., 1995).

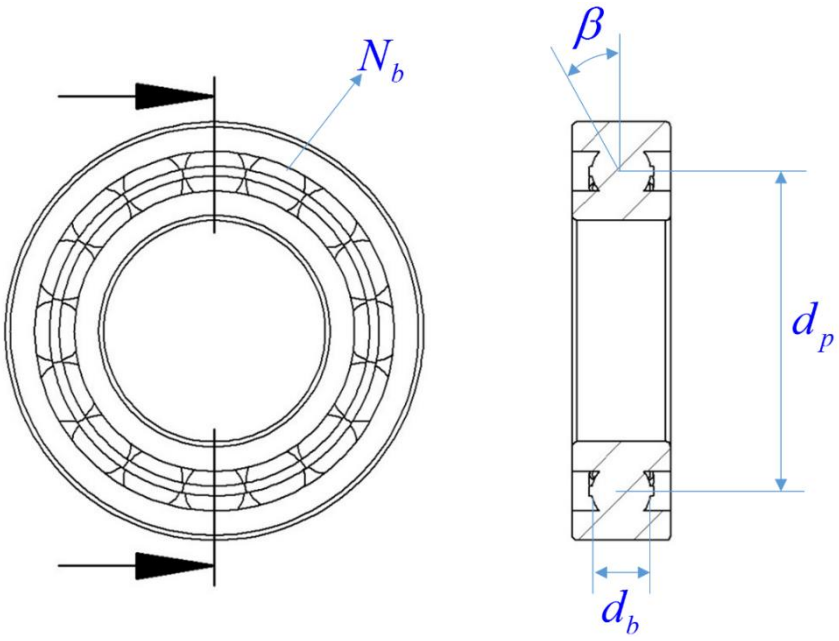

Figure 2.1. Ball bearing geometry

3. EXPERIMENTAL SETUP AND DATA ACQUISITION

In this thesis, current, vibration and acoustic data are acquired for feature extraction and fault classification. The experiments were set up under a self-designed test rig on which a single-phase permanent magnet synchronous generator and a test motor coupled to it are placed. By adjusting the resistance values of the resistor load bank which is connected to the output of the single-phase 4.2 kVA permanent magnet synchronous generator, the different loading conditions of the test motors can be arranged. All test motors are identical and products of trademark GAMAK, 3-phase and 2-pole squirrel cage induction motors rated at 2.2kW, 50Hz, $380V_{LL.}$ Power factor of the test motors is 0.82 and rated current of the test motors is 4.94 A. A Δ-Y connected 25 kVA isolation transformer is located between the AC network and the test rig.

Data acquisition processes are conducted at Power Systems Laboratory of Anadolu University Electrical and Electronics Engineering Department. Different experiments are realized by induction motors directly supplied with the output of the isolation transformer located between AC network and the test rig. Furthermore, in order to observe the effect of the adjustable speed drives (ASD) on supply current, some current acquisition experiments are realized by placing an industrial adjustable speed drive. A rough scheme of the experimental setup for adjustable speed drive case can be seen in Figure 3.1.

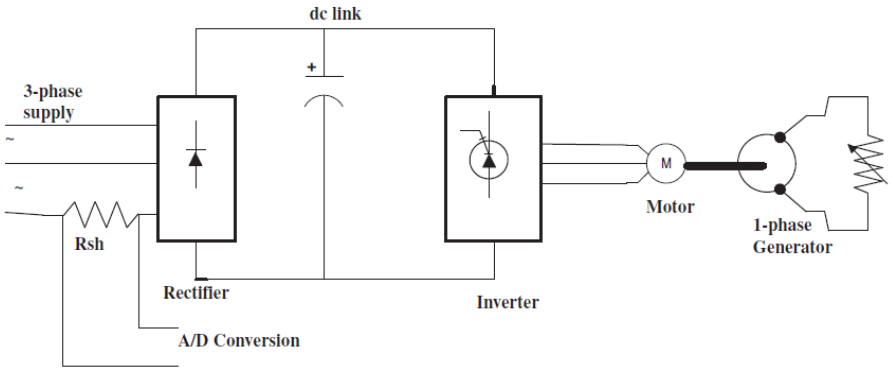

Figure 3.1. Current acquisition of test motor driven by an adjustable speed drive

The adjustable speed drive 3-phase, product of trademark Enko model CN2211 and placed between the output of the isolation transformer and the terminal box of the test motors. By placing ASD to test circuit, motors are able to operate at constant speeds arranged by the speed reference of the inverter. In previous works with the current data acquired in the same testing environment, very successful classification ratios are achieved in the direct AC supplied case of the motors (Ece and Gerek, 2006; Günal et al., 2009). But in the case of placing an ASD to test procedure, due to the pulse-width modulation (PWM) switching of the voltage source inverter, the motor current waveforms can be obstructed by the noise-like additive waveforms, which make fault classification from stator current more challenging. From this motivation, current acquisition is realized both with direct AC driven case and ASD driven case of the test motors.

For the experimental verification, frequently encountered mechanical and electrical faults are created synthetically on five of these test motors. In order to make clear comparisons, one of these identical motors is left untouched to get healthy motor data. The list of motor faults created synthetically and their assigned classes can be seen in Table 3.1.

Table 3.1. List of synthetically created faulty motors in experimental setup

Class	Faulty Motor
rb1	Motor with bearing fault type-1
rb2	Motor with bearing fault type-2
rot3	Motor with 3 broken bars
rot5	Motor with 5 broken bars
sw	Motor with arbitrarily shorted stator winding
healthy	Healthy reference motor

The synthetically created fault types are chosen such that those are the most encountered incipient faults in industry. Broken rotor bar faults are realized by punching holes to the rotor bars with a drill which can be seen in Figure 3.2. Three and five holes are drilled respectively to two different motors over total 18 rotor bars.

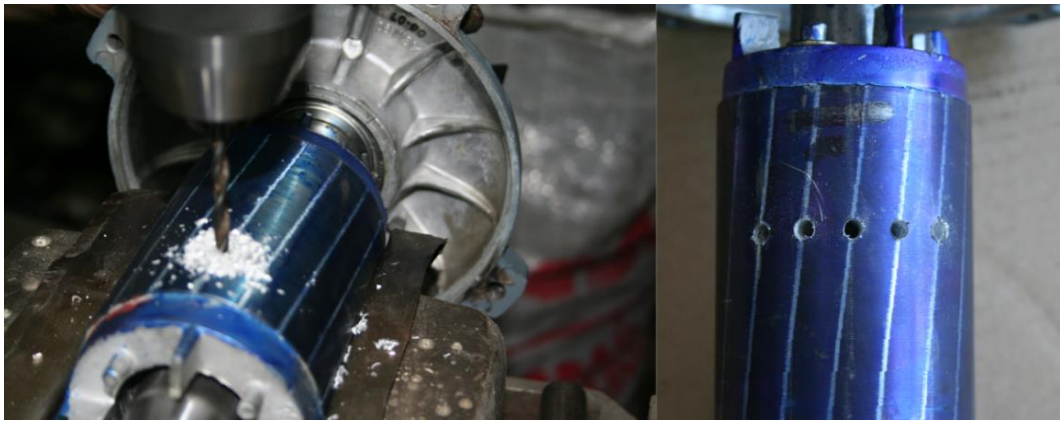

Figure 3.2. Realization of broken rotor bar fault

In order to simulate bearing related faults, bearings of the unused motors are disassembled and replaced with faulty bearings. Faulty bearings are obtained from a real industrial induction motor maintenance workshop which are disassembled from induction motors that had been used for a long time and are taken out of service due to the noise and excessive heat problems. The faulty and unused bearings can be seen in left and right sides of the Figure 3.3 respectively.

Figure 3.3. Faulty and unused bearings

Shorted stator winding fault is created by arbitrarily peeling the insulation of two adjacent stator coils of another unused test motor for a couple of millimeters and soldering them together.

In industrial applications, induction motors are mostly driven directly from AC network with constant voltage and frequency under various loads. To simulate different loading conditions, test motors are coupled with a single-phase 4.2 kVA permanent magnet synchronous generator connected to an adjustable resistive load bank. The resistor values on load banks are adjusted to different values such that the motors are driven by different levels of stator current which corresponds to a different loading condition. These values are selected such as 3.6, 4.1, 4.7, 4.9, 5 and 5.4 Amperes. By selection of these values, the situations of motors operating below and above the rated current values can be simulated. Before collecting the data, test motors start to operate under no load and after a few minutes of operation. When the motor reaches to the steady state, the resistor values have been adjusted to load the motors consecutively to the pre-determined load levels during the experiments.

3.1. Acquisition of Stator Current Data

Current acquisition is realized both with direct AC driven case and ASD driven case of the test motors. In directly driven case, motors are driven with the output of the isolation transformer. In this case, motor speeds are slightly changing due to the concept of rotor slip. In ASD driven case, motors are supplied from the output of adjustable speed drive which is located between the output of the isolation transformer and the test rig. In this case motors are operated at constant speeds which is determined by the frequency reference of the ASD.

The 3-phase supply-side stator currents are obtained via properly selected shunt resistances located at supply side and Sony Tektronix A6906 isolators. Current data are digitized with an NI 6251 data acquisition card with 16 bit vertical resolution at a sampling rate of 20 kHz. The acquired supply side current and corresponding motor side current waveforms obtained from test motor with 5 broken bars (rot5) driven by adjustable speed drive with 35 Hz speed reference can be seen in upper and lower side of the Figure 3.4 respectively.

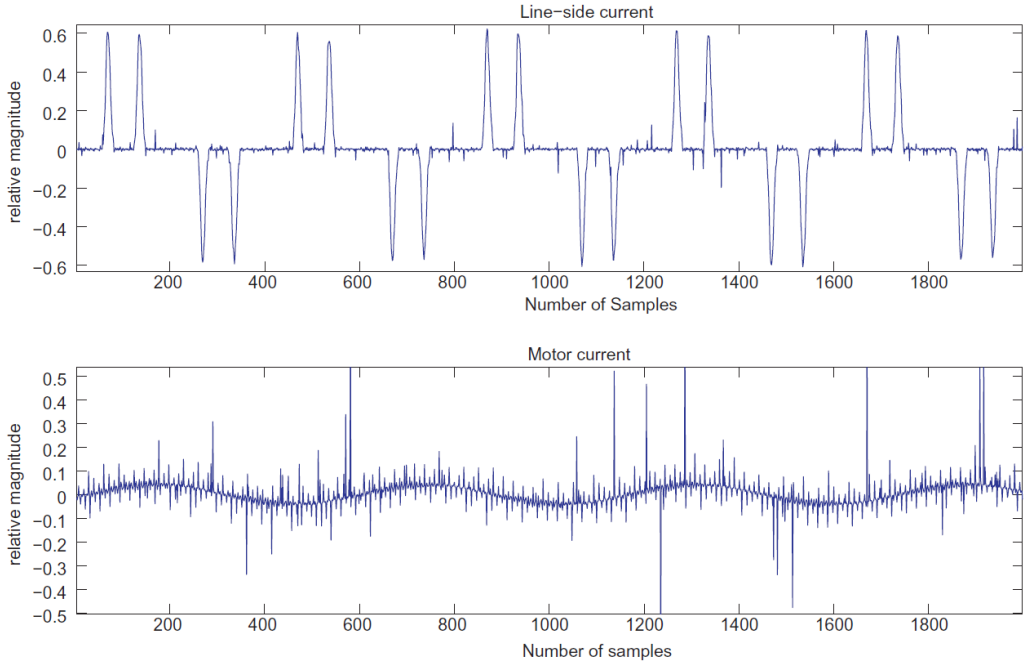

Figure 3.4. Line-side and motor current waveforms

An expert inspection of these waveforms shows that due to pulse-width modulation (PWM) switching of the voltage source inverter, the motor current waveform with 35 Hz fundamental is occluded by the noise-like additive waveform typically above 10 kHz. When this motor current waveform data is used to extract necessary features for fault detection and classification, pre-process of the data is needed. First, proper filtering to eliminate noise due to the PWM should be applied and then the fundamental frequency of the inverter output which is the speed reference for the motor under test should be measured. On the other hand, although it is not a sine wave and drawn during equal fractions of each half cycle due to the large dc link capacitor, supply-side current is always at the known fundamental frequency of the supply and is noise free due to the front-end diode rectifier. Therefore, supply-side current data is used since our initial experiments revealed that it contains required information for fault detection and classification and does not require any pre-processing. Forty seconds-long data is obtained from all six motors for each loading conditions at three speed references, (35, 40 and 50 Hz) which result in digitized data files of size 800,000 samples.

3.2. Acquisition of Vibration Data

Vibration data are obtained from the case in which induction motors are supplied directly from the AC network. An integrated electronic piezoelectric (IEPE) accelerometer, product of trademark Metra Mess model KS943B.100 is used for vibration sensing. The accelerometer has a magnetic base for placing to the motor fan cover, which can be easily mounted and removed. The accelerometer is connected to a multichannel signal conditioner, model M108 of the same brand, for amplifying the vibration signals. Signals are digitized with an NI 6251 data acquisition card with 16 bit vertical resolution at a sampling rate of 20 kHz. Vibration data are collected from 5 test motors under 6 different pre-determined loading conditions for forty seconds. For accuracy of the experiments, the placing position of the accelerometer set constant to each test motor. The accelerometer and its position on fan cover of one of the motors can be seen in Figure 3.5.

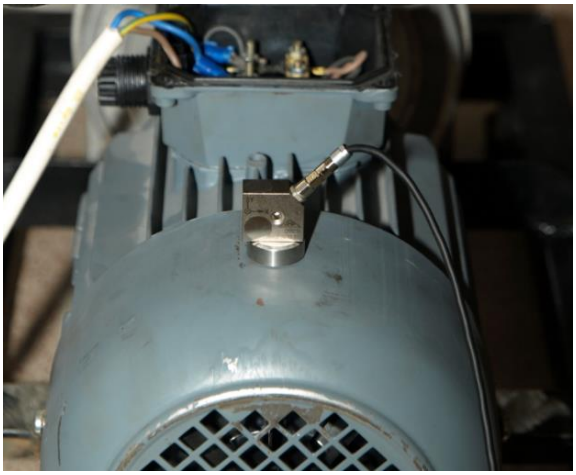

Figure 3.5. Accelerometer and its position on fan cover of the motor

Besides vibration data, acoustic data is also collected from induction motors. Since the data acquisition processes are handled with different appliances and PCs at different sampling frequencies, simultaneous recordings do not exist. Acoustic and vibration data were able to be recorded at the same environment with some small time delays.

3.3. Acquisition of Acoustic Data

Acoustic data are acquired in laboratory environment with ambient noise via five microphones surrounding the test rig. At each pre-determined current level, approximately 30 seconds of operating sound recordings are collected by five microphones which are located around the test rig and via a full transparent analog amplifier at a sampling rate of 44.1 kHz. The location of the microphones can be seen in Figure 3.6.

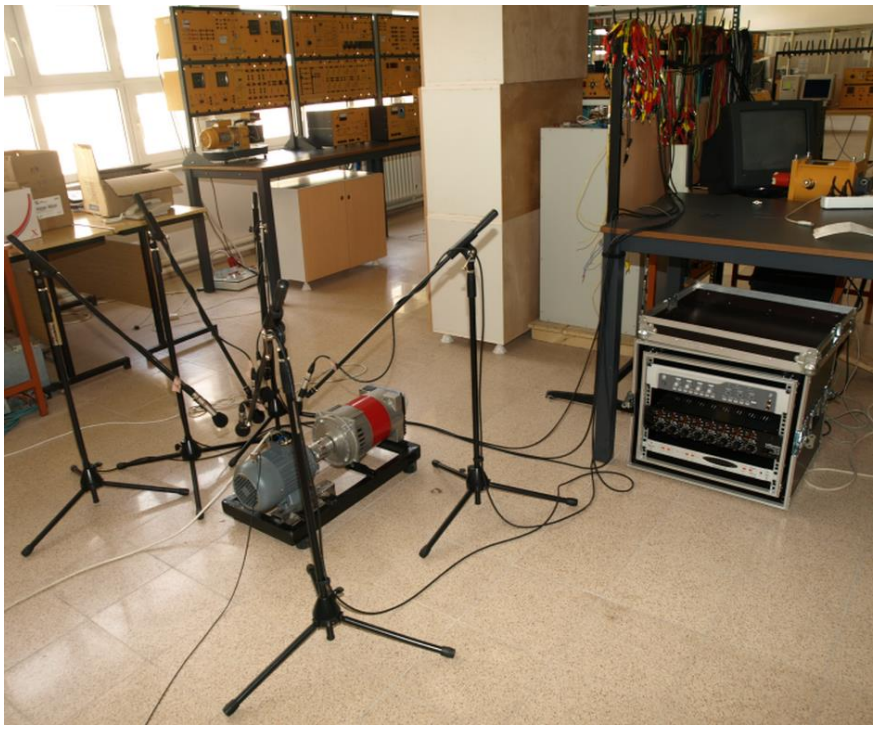

Figure 3.6. The placement of the microphones over test rig

One of these microphones is located around 60 centimeters above the center of the test rig. Other remaining four microphones are located at a lower height compared to the center microphone and they are placed to mark the edges of a rectangular shape, which surrounds the test rig. The locations of the microphones are very important when calculating the cross correlations between microphone pairs. This placement of microphone array produces a virtual hemisphere that covers all the experimental setup.

All the experiments are deliberately carried out in a noisy environment to simulate real working environment on purpose and the average ambient sound pressure level (SPL) is recorded as 53.2 dB, which can be considered as quite noisy environment. Sound pressure levels related to each five of the test motors during experiments is given in Table 3.2.

The microphones are directional and cardioid type condenser ones and they are connected to an analog microphone preamplifier product of the trademark Millennia model HV-3D. The sound data are digitized with a sampling frequency of 44.1 kHz, which results in digitized files of containing approximately more than a million samples for each recording.

Table 3.2. Sound pressure levels of the three experiments of the dataset

Environment SPL : 53.2 dB

		Loading Conditions						
		3.6 A	4.1 A	4.7 A	4.9 A	5 A	5.4 A	
Healthy Motor	Exp1	73.8	76.5	78.5	78.5	78.5	79.4	dB
	Exp2	74.9	76.1	74.6	75.1	76	75.4	dB
	Exp3	73.8	73.8	73.8	73.8	73.8	72.6	dB
Stator Winding Fault (sw)	Exp1	75.4	74.7	74.5	74.6	74.1	74.1	dB
	Exp2	74.1	73.8	74.1	74.4	73.8	74.2	dB
	Exp3	74.8	74.4	74.8	74.4	73.8	74.7	dB
Rotor Bar Fault (rot3)	Exp1	75	76.1	77.1	77.1	78.1	77.1	dB
	Exp2	76	74.5	75	75	75.4	74.5	dB
	Exp3	75	74.5	74.1	74.1	74.2	73.8	dB
Rotor Bar Fault (rot5)	Exp1	80	78.8	79.1	79.1	78.5	79.1	dB
	Exp2	78.8	80.1	79.5	79.5	79.5	79.5	dB
	Exp3	76	75.4	76.1	76	76	76	dB
Bearing Fault (rb1)	Exp1	84.6	83.7	83.3	83.2	83.2	83.2	dB
	Exp2	83.2	83.2	83.2	83.2	83.2	83.2	dB
	Exp3	83.2	83.7	83.4	83.4	83.8	83.2	dB
Bearing Fault (rb2)	Exp1	86.2	84.5	84.2	84.3	84.2	84.2	dB
	Exp2	83.7	83.7	83.2	84.2	83.2	82	dB
	Exp3	83.2	83.2	83.4	83.7	83.2	82	dB

These recording procedures are repeated three times for each test motor by dissembling the motor from the test rig and reassembling it on to simulate mounting differences which can be caused by the technical staff in real industrial work platform. In order to fix the motor on to the test rig, mechanical parts like screws and bolts are used and in each different assembling attempt, the alignment of the connection may change and it may show its own mechanical characteristics which may alter noise level and vibration characteristics. In this way, different cases corresponding to differently aligned test bed possibilities which can physically effect the acoustic and vibration data are handled to create more advanced benchmark database to build a more reliable fault diagnosis system. The aim of differentiating the faults in this manner during multi experiments is to certify the proposed methods more accurately.

4. FEATURE EXTRACTION

In this thesis, different feature extraction methods are proposed and applied to the current, vibration and acoustic signals that are obtained from the laboratory environment.

4.1. Feature Extraction by Calculating Wavelet Packet Decomposition Coefficients of the Current Data

Wavelet transformation of signals to solve various real-life problems are widely used tool in many engineering fields. In wavelet packet decomposition (WPD) of a signal, the signal is filtered with both low-pass (LP) and high-pass filters, whose cutoff frequencies are one fourth of the sampling frequency of the signal (Eren and Devaney, 2004). The LP and HP filtered signals are half size of the original signal that represents the low frequency and high frequency contents of the signal and called the approximation (A) and the detail (D) respectively. If this decomposition procedure is applied to the first layer approximation and detail signals, a new level of decomposition is achieved which consists of four signals named as AA (approximation of the approximation), DA (detail of the approximation), AD (approximation of the detail), and DD (detail of the detail), each of which are in the size of one fourth of the original signal (Ocak et al., 2007). In the same manner, this decomposition process can be iterated to more levels until the decomposition reaches the desired frequency resolution (Akansu and Haddad, 2001).

Time domain waveform plots of the supply-side current for ASD healthy reference motor and ASD-faulty motors were acquired at sampling rate of 20 kHz and are illustrated in Figure 4.1. By visual inspection of these waveforms, it can be seen that they are quite similar and seem to have similar properties and it is hard to discriminate from each other. As a result, direct use of these waveforms is not suitable in detection and classification of motor faults.

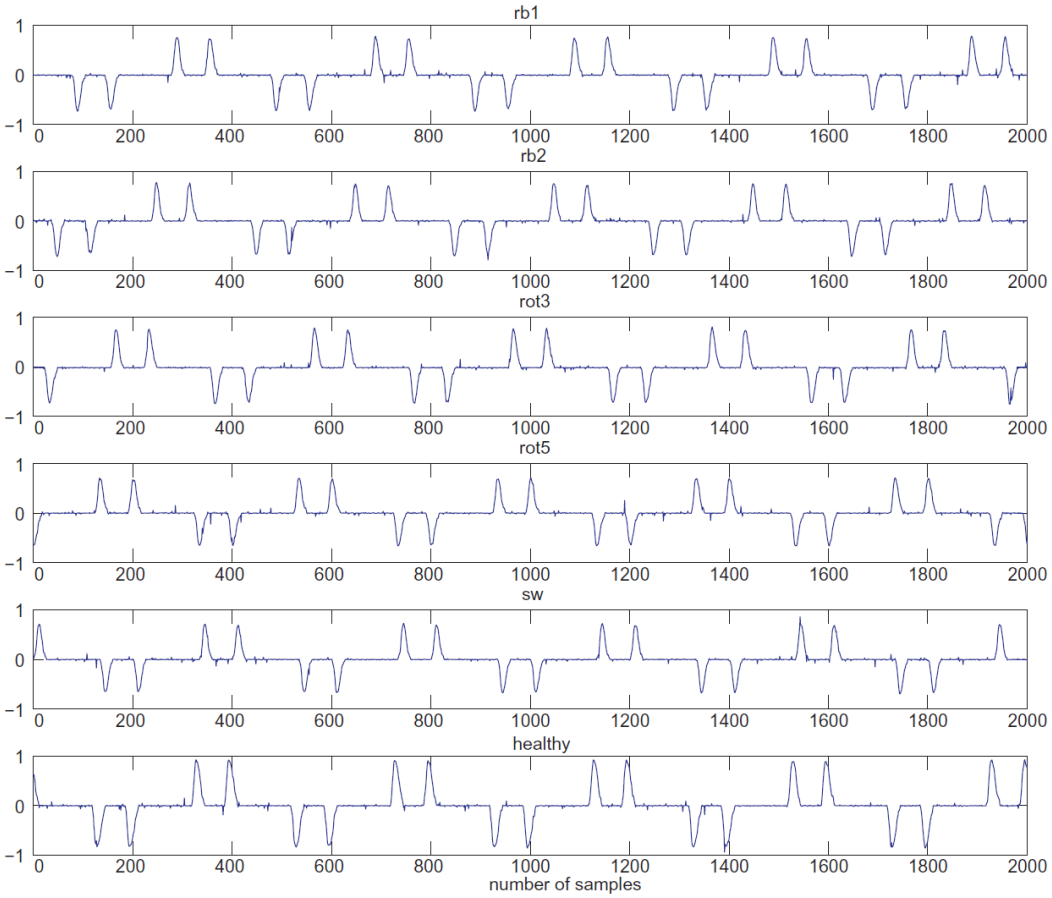

Figure 4.1. Supply-side current waveforms of test motors driven with ASD under 4.1.Amperes load at 40 Hz speed reference

Induction motor faults, especially broken rotor bars, are known to cause elevated sidebands around the fundamental frequency component in the spectrum of motor stator current (Loránd et al., 2004). The location of these side bands are seriously affected by the loading condition and tend to become closer to the fundamental frequency especially when the motor load is low below than the rated current. Therefore extracting the information related to the changes in side-bands requires to monitor very narrow frequency regions of the entire spectra. Consequently, a very high frequency resolution is needed in order to monitor such narrow frequency regions. If Fast Fourier Transform (FFT) were to be used in this work, entire length of each data set (800,000 samples) must be used in FFT and later regions of interest may be extracted from the entire spectra to obtain a high

frequency resolution. On the other hand, using wavelet packet decomposition with properly selected number of levels and filter type would provide better frequency resolution compared to the FFT, while requiring less number of data samples. Also, to calculate all branches and nodes of the WPD coefficients is not necessary since the frequency region of interest is known to be around the fundamental frequency. Careful selection of number of data samples, filter size, and decomposition level is essential in using WPD. A schematic representation of the 11th level of WPD can be seen in Figure 4.2. If the size of the data is not necessarily long, as the number of decomposition level increases and data is down sampled at each successive level, remaining length of data samples at some nodes would become less than the selected filter size resulting meaningless convolution of data samples with filter coefficients. The examples of selection different filter types and their effect on the classification is showed on results section.

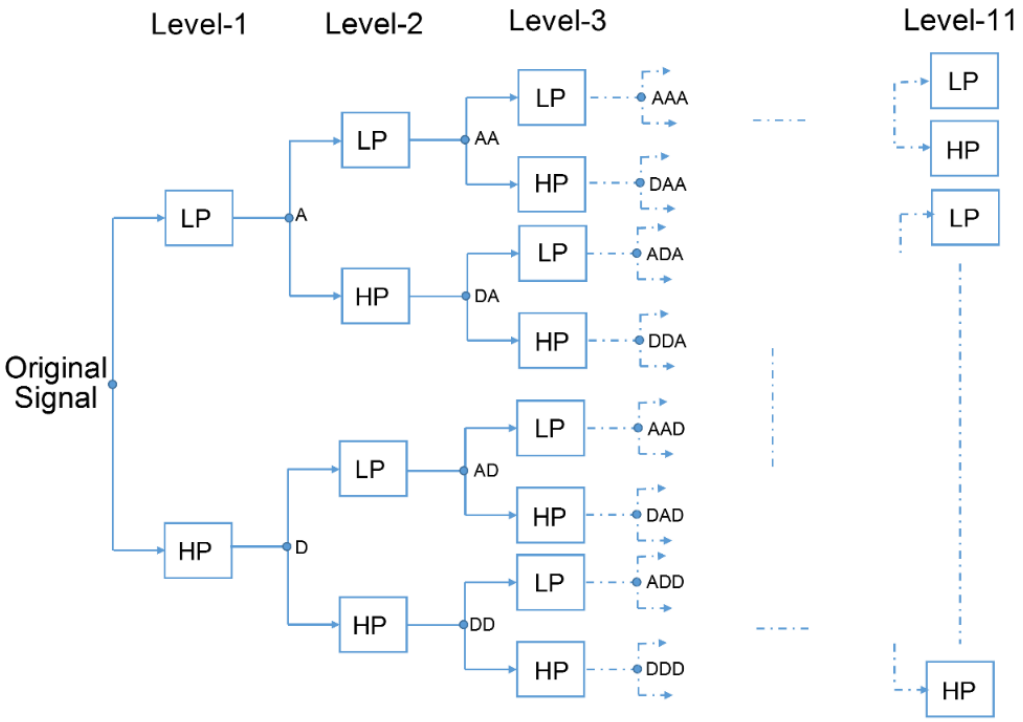

Figure 4.2. 11th level of wavelet packet decomposition of the original signal

In this work, acquired data, sampled at 20 kHz, is analyzed using 11th level of WPD. This way, the coefficients of three nodes at the 11^{th} level of decomposition, which corresponds to 43.92–48.8 Hz, 48.8–53.68 Hz, and 53.68–58.56 Hz frequency bands that covering the region (43.92–58.56 Hz) of both side-bands and the 50 Hz fundamental frequency are obtained.

Using the coefficients of each node, four fundamental statistical signature identifiers are calculated resulting 12 element feature vectors. The signature identifiers are mean, standard deviation, skewness, and kurtosis of each of the three nodes mentioned above. Hence, from each acquired data from ASD-motor combination, 40 feature vectors with 12 elements were obtained at each load condition and at each speed reference frequency. These four signature identifiers, mean, standard deviation, skewness, and kurtosis denoted as *F1*, *F2*, *F3* and *F4* respectively, can be mathematically explained as follows:

$$F1 = \mu_x = \frac{1}{N}\sum_{i=1}^{N} x_i \tag{4.1}$$

$$F2 = \sigma_x = \sqrt{\frac{1}{N}\sum_{i=1}^{N}(\mathrm{x}_i - \mu_x)^2} \tag{4.2}$$

$$F3 = \frac{\left[\frac{1}{N}\sum_{i=1}^{N}(\mathrm{x}_i - \mu_x)^3\right]}{\sigma_x{}^3} \tag{4.3}$$

$$F4 = \frac{\left[\frac{1}{N}\sum_{i=1}^{N}(\mathrm{x}_i - \mu_x)^4\right]}{\sigma_x{}^4} \tag{4.4}$$

where N is the number of WPD coefficients in each node, μ_x is the mean, σ_x is the standard deviation of the coefficients of each node, respectively. If x_i is the i^{th} coefficient, skewness *(F3)* and kurtosis *(F4)* elements are calculated for each node as given above.

4.2. Feature Extraction by Calculation of the Cross Correlation of the Acoustic Data

The next feature extraction technique proposed in this thesis is calculating the cross correlations of the acoustic data recorded by the microphone pairs. According to the nature of the fault, the mechanical and the electrical motor faults cause irregular air-gap flux that affects spinning of the rotor. According to this irregularities and effects of the faults to the proper working conditions, the amplitude of fundamental frequency and its related sideband artifacts show variations according to the placements of microphones (Germen et al., 2010). It is important that, the characteristic of recorded acoustic data differs in each microphone according to its distance to certain parts of the motor. The interrelation between the channels of semi-sphere shaped located microphone array placed over the motor is also changed due to these discrepancies on the operating sound. Besides, types of faults are supposed to differentiate channel interrelationships. In order to classify different motor faults, cross-correlation coefficients between microphone channels are used as attributes of the feature sets. For calculation of the cross correlation coefficients, Pearson product-moment correlation coefficient method, which is defined with the equation (4.5), is applied to the recorded digitized acoustic data by microphone pairs (Lee Rodgers and Nicewander, 1988).

$$r_{x_i x_j} = \frac{\sum_{n=0}^{N-1}\left[(x_i(n)-\overline{x_i})(x_j(n)-\overline{x_j})\right]}{\sqrt{\left[\sum_{n=0}^{N-1}(x_i(n)-\overline{x_i})^2\right]\left[\sum_{n=0}^{N-1}(x_j(n)-\overline{x_j})^2\right]}} \tag{4.5}$$

In equation (4.5), subscripts i and j denote the indices of microphones, x_i and x_j are their corresponding data array and N is the number of samples in these arrays, which is taken as 800000 in this work. Since five microphones are used, the number of total possible combinations of microphone pairs among five channels is ten, ten different cross correlation coefficients can be calculated. These ten features which are shown on Table 4.1 are obtained from these cross correlation coefficients

and they are added to the overall feature set for some of the acoustic based classification experiments.

Table 4.1. Cross-correlation features of acoustic data recorded by microphones

Cross-Correlation Features				
#1: $r_{\chi_1\chi_2}$	**#2**: $r_{\chi_1\chi_3}$	**#3**: $r_{\chi_1\chi_4}$	**#4**: $r_{\chi_1\chi_5}$	**#5**: $r_{\chi_2\chi_3}$
#6: $r_{\chi_2\chi_4}$	**#7**: $r_{\chi_2\chi_5}$	**#8**: $r_{\chi_3\chi_4}$	**#9**: $r_{\chi_3\chi_5}$	**#10**: $r_{\chi_4\chi_5}$

4.3. 2D Discrete Wavelet Transformation Based Feature Extraction from 2D Grayscale Image Representation of the Data

Texture as an important characteristic for the analysis of many types of images is being used for many applications (Ojala et al., 1996). Various measures derived from texture properties for classifying texture have been proposed in literature (Van Gool et al., 1985; Tuceryan and Jain, 1993). Any one dimensional data can be converted into two dimensional image data by normalization and proper partitioning of the original data, on which texture related measures can be applied.

This feature extraction method is an indirect one, which uses two-dimensional (2D) grayscale images obtained from current, vibration and acoustic data. The 2D image representation of one dimensional data became popular recently in pattern recognition and signal processing and also has great potential in detecting power quality events (Ece and Gerek, 2004; Gerek and Ece, 2004). During the conversion process of 1D data to 2D grayscale image, the amplitude of each data samples are normalized between 0 and 255, which is the range for grayscale, and these normalized values become the pixel intensities.

When directly supplied with AC source, induction motors rotate very close but a bit slower than the synchronous speed also level of loading alters the rotation speed. The rotation speed of the motor slowly decreases with the increase of the stator current. Thus, determination of the exact real rotor frequency is complicated and has great importance while constructing 2D images from 1D data. In this work,

the widths of the grayscale images are determined due to the length of samples of a complete period of the signal. Since the sampling frequency of the acoustic data is 44.1 kHz, and motor fundamental frequency is 50 Hz, for each complete cycle, 882 samples are necessary to cover a complete period of the signal under no-slip case. But in practice, the fundamental frequency component changes and it becomes less than 50 Hz. In these kinds of situations, it is necessary to use more samples than 882 to cover a complete period of data.

In 2D grayscale image construction process from one dimensional data, first the normalization between 0–255 is realized. Then the first element of normalized data is assigned as the first pixel value, which is the top-left corner of the image. The succeeding elements are assigned to the right of first pixel until the elements are rendered to form one row consisting of a complete period. After the assignment of the last pixel in the first row, the same procedure is carried out for the next row and this process is repeated until *mxn* sized images are obtained. This process is depicted in Figure 4.3.

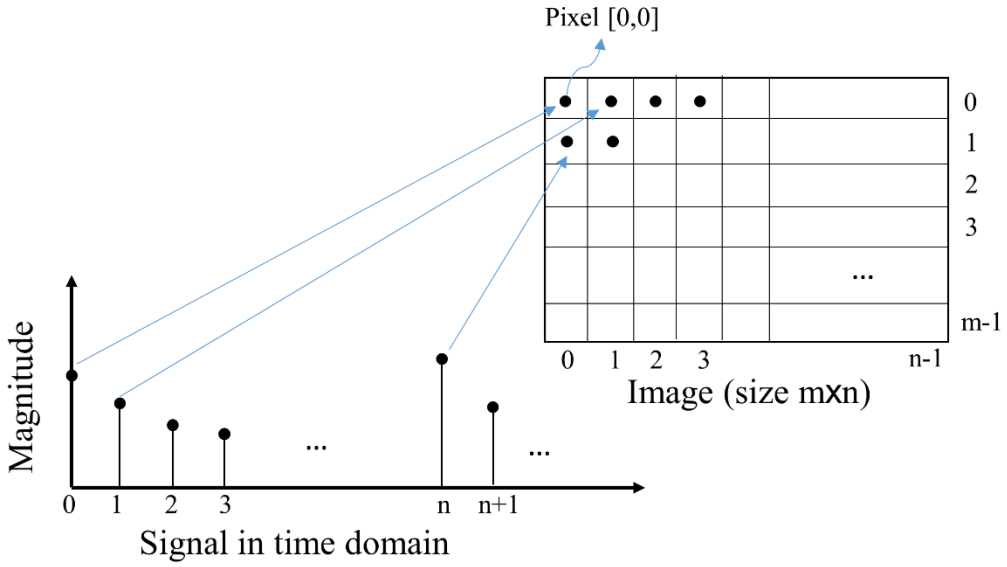

Figure 4.3. Signal to image construction scheme

In this thesis, square shaped grayscale images are preferred and *nxn* sized grayscale are constructed from 1D data.

When constructing the 2D grayscale images containing non-overlapping period segments, determination of the sample size of a complete period is crucial. Hereby, this problematic issue is solved by finding the autocorrelation peaks of the 1D data, which indicate the ends of complete oscillation cycles. The autocorrelation values of the acoustic data recorded by all microphones are the same for specific motor type under same loading condition. This situation can be seen by inspecting Figure 4.4, where the first 2000 samples of autocorrelation sequences of the five microphone recordings for healthy motor under loading condition of 3.6 Amperes are depicted.

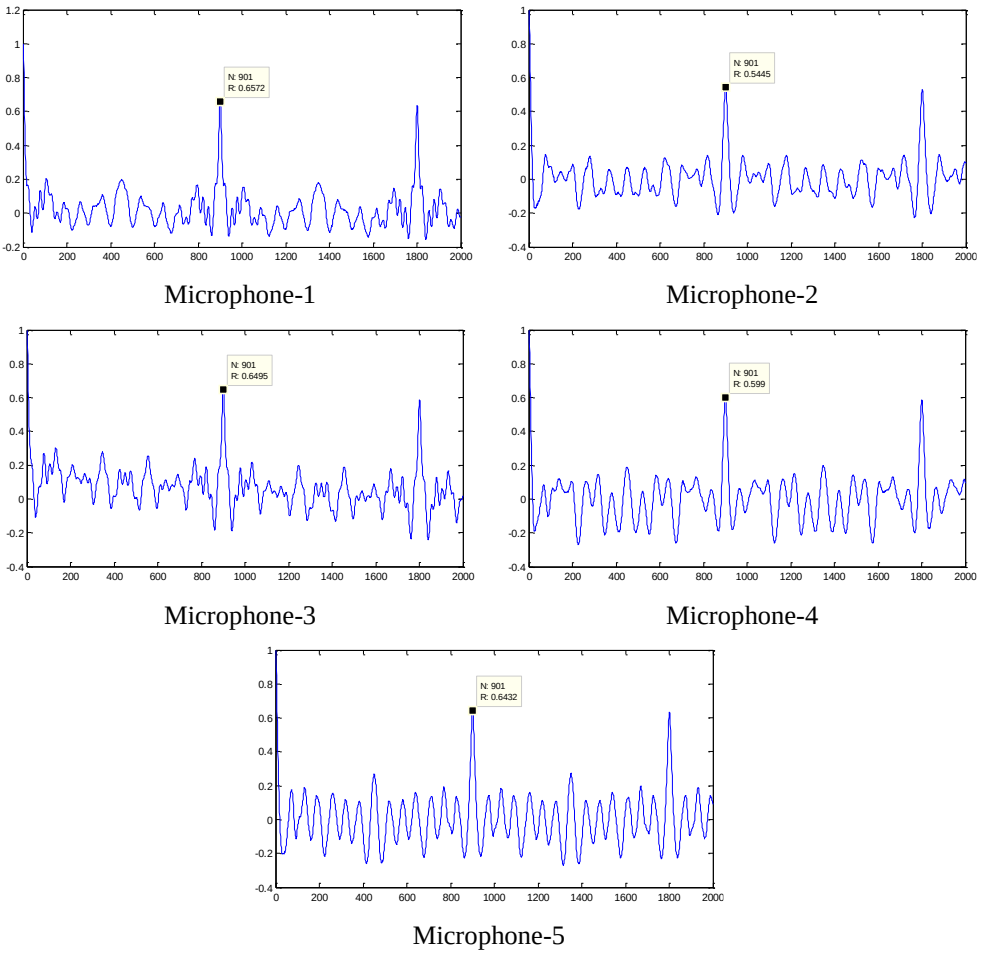

Figure 4.4. Autocorrelation sequences of the five microphone recordings for healthy motor under 3.6 Amperes load

If the test motor changed, even under the same loading condition, the size of the samples which consists of a complete period changes due to fault type. The first 4500 samples of autocorrelation sequences of the acoustic data of the test motors operated under 3.6 Amperes stator current, recorded by the first microphone can be seen in Figure 4.5.

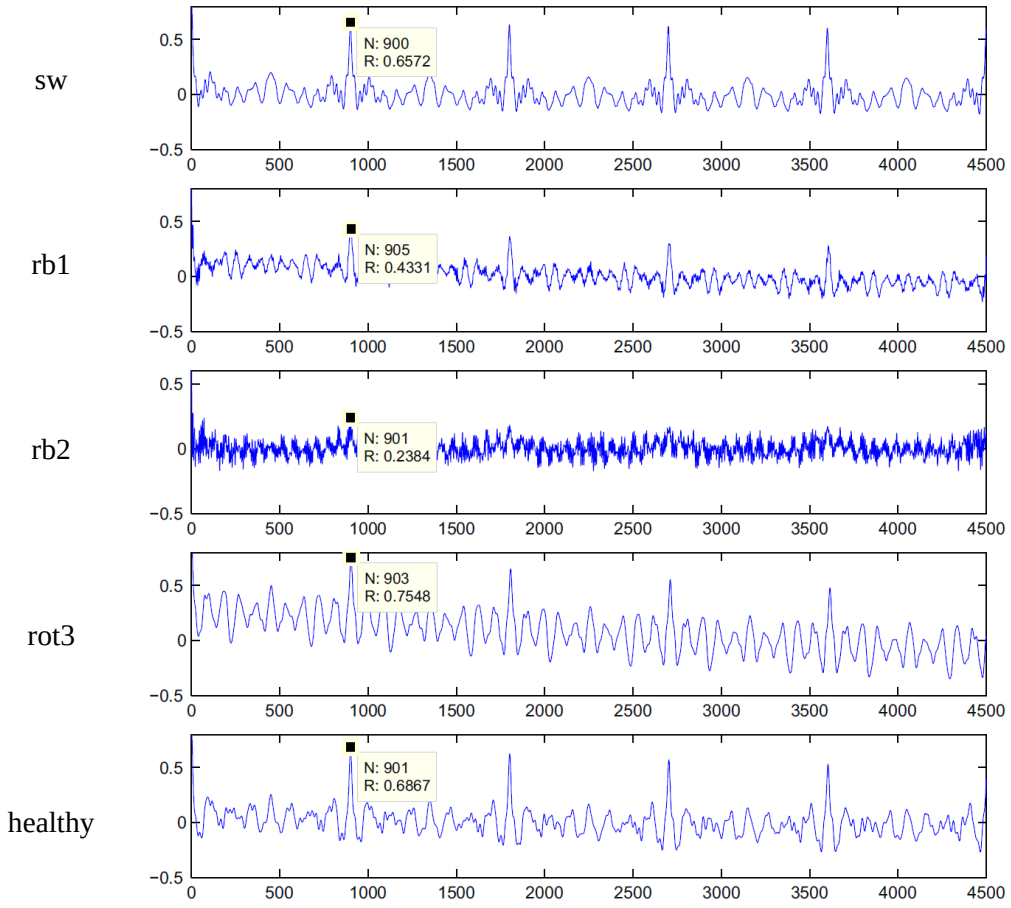

Figure 4.5. The autocorrelation sequences of the test motors operating under 3.6 Amperes load recorded by first microphone

It is clearly seen that motors with different types of faults have different autocorrelation peaks which alters the size of created grayscale images. The cycle values at different loading conditions are also calculated in the same manner for current and vibration data. As an example, the results for sample sizes of a single complete period of 1D acoustic signal acquired from test motors having different

types of faults at each loading conditions calculated by autocorrelation peaks for each test motor are given in Table 4.2.

Table 4.2. Sample sizes of a period of the acoustic data of the test motors running under different loading conditions

	3.6 A	4.1 A	4.7 A	4.9 A	5.0 A	5.4 A
sw	900	906	912	914	916	919
rb1	905	910	914	917	918	921
rb2	901	907	908	916	919	923
rot3	903	910	912	919	922	926
healthy	901	906	913	914	915	920

The image representations of the acoustic data recorded from the test motors under 3.6 A by the first microphone are shown in Figure 4.6. The 2D image creation process is carried out for every separate five microphones for test motors under six different loading conditions for three different experiment trials. Since the images preferred to be square shaped, the acoustic image database consists of grayscale square images whose widths ranging 900 to 926 according to their corresponding autocorrelation peak values.

In order to extract another set of features, single level 2D discrete wavelet transformation (DWT) is utilized to the grayscale images in test database. The discrete wavelet transformation is the projection of a signal onto two subspaces called the approximation and the detail subspace. By iteratively applying DWT to the approximation, a series of approximation and detail spaces can be obtained. Projection process is accomplished by discrete time sub-band decomposition of input signals using low-pass and high-pass filtering operations followed by down-sampling by 2. First the low-pass and high-pass filters and the down-sampling by 2 operations are applied along rows of an *nxn* 2D square shaped image. After this step, the outputs of the process are two sub-images, denoted as L and H, with sizes *nxn/2*. Then, the same procedure is applied along the columns of these newly obtained sub-images L and H.

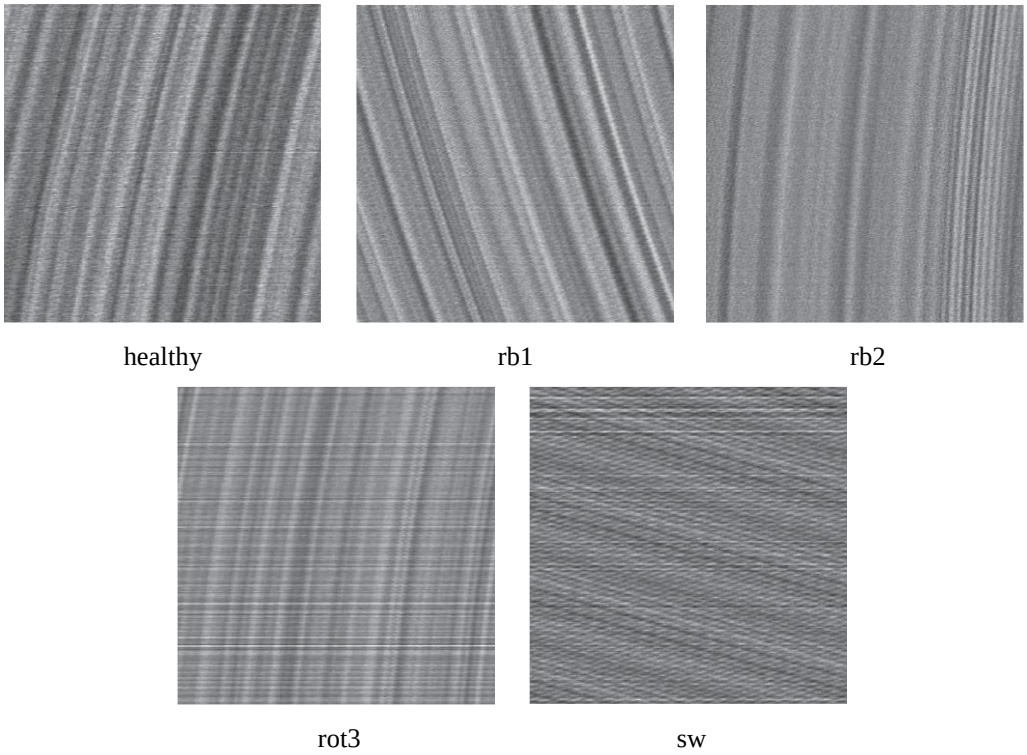

Figure 4.6. 2D image representations of acoustic data recorded from first microphone over five different test motors under 3.6 Amperes loading condition

The outputs at the second step are four square-shaped grayscale images having size of *n*/2x*n*/2. These two steps correspond to single-level discrete wavelet transform of the image. The output images are called the energy, vertical, horizontal and the diagonal sub-images and denoted as LL, LH, HL and HH respectively.

The energy image (LL), which is also called the approximation image, resembles the original image. Remaining images show great differences which contain more complicated textures. Clearly, it can be inferred that, these textures may show close relationship with the traces of motor failures and they provide great opportunity for feature extraction related to fault type. The four sub-images constructed after single level 2D wavelet decomposition of the healthy motor image which can be seen in the left top of Figure 4.6, are demonstrated in Figure 4.7.

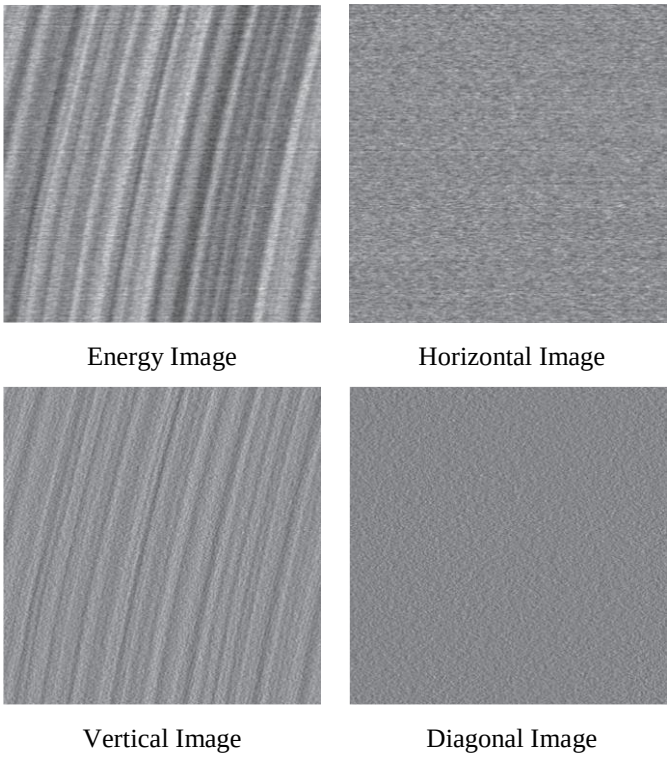

Figure 4.7. The sub-images constructed after one level 2D wavelet decomposition of the healthy image shown in the left top of Figure.4.6

These sub images have different textures which serves a great medium for extraction of texture related features. Figure 4.8 consists of zoomed versions of vertical images of the 5 different motor types recorded by first microphone under 3.6 A loading condition.

In wavelet decomposition, the selection of the wavelet type affects the process. Various types of wavelet filters such as coiflet, morlet and several types of filters from Daubechies family are used in the experiments of the thesis work but db2, which is also called as Haar filter, succeed fairly well when compared to others. Since this filter has very simple structure, for the minimum computational cost, it is preferred in filtering process of the decomposition.

In the equations (4.6) and (4.7), mother wavelet $\psi(t)$ and the scaling function $\phi(t)$ of Haar wavelet can be seen.

$$\psi(t)=\begin{cases}1 & 0\le t<1/2\\ -1 & 1/2\le t<1\\ 0 & otherwise\end{cases} \tag{4.6}$$

$$\phi(t)=\begin{cases}1 & 0\le t<1\\ 0 & otherwise\end{cases} \tag{4.7}$$

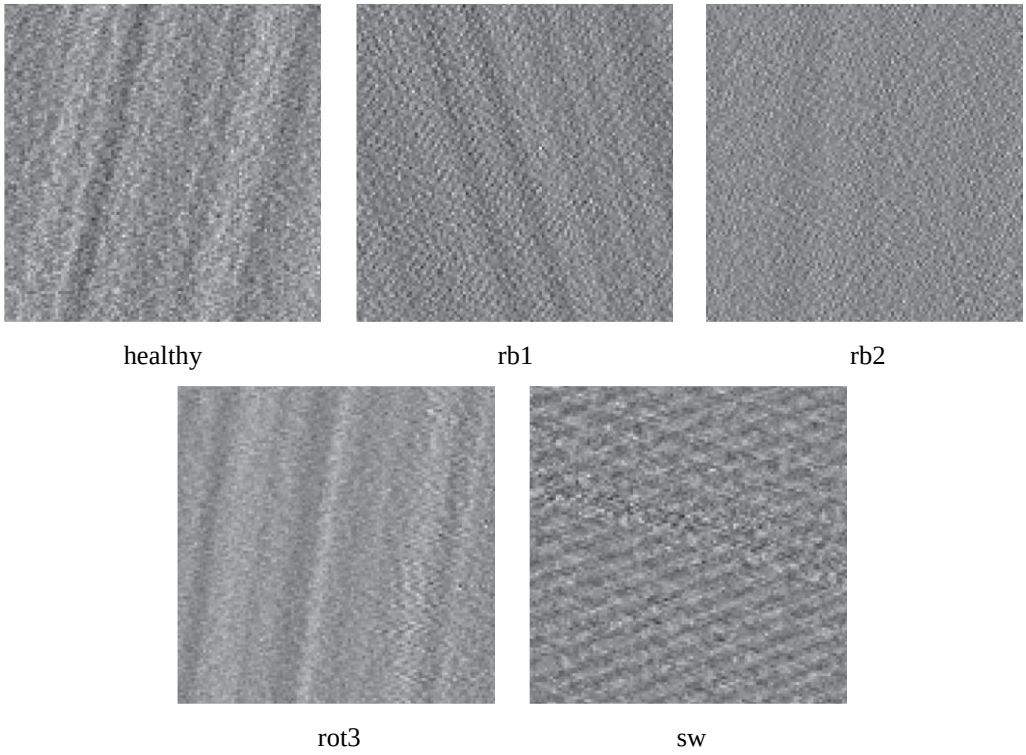

Figure 4.8. Zoomed vertical images of the five different test motors types recorded by first microphone under 3.6 Amperes loading condition

After single level 2D wavelet transformation process, six different features are extracted from four sub-band images. First two of these features are the root mean square energy of the vertical and diagonal images. Remaining features are acquired by calculating the mean of row correlations of the horizontal image and the mean of the column correlations of the vertical, diagonal and energy images. The correlations between two adjacent rows or columns are calculated over the sub-images and the mean of these calculated values are taken as the feature. Detailed analysis of the images acquired by wavelet decomposition reveals that the most

distinguishable information is located mostly in their columns compared to the rows. The main reason of this situation arises from the fact that, the rows approximately consisted of the data samples of one period of the data. Consequently, there are no distinguishable differences between rows. However, according to this periodicity, the column information contains the possible distinguishable characteristics of the artifacts caused by faults and focusing on this data would be more informative. It is worth to state that, both in vertical and diagonal images, the textures conceal the indications of the faults, since the column information is mostly contained by vertical and diagonal images.

Equation (4.8) is used for the calculation of the mean of cross-correlation coefficients among neighbor columns within the image, where *N* and *M* denote number of columns and rows respectively.

$$r_{column} = \frac{\sum_{j=0}^{N-2}\left(\frac{\sum_{j=0}^{M-1}\left[\left(I(i,j)-\overline{I(\cdots,j)}\right)\left(I(i,j+1)-\overline{I(\cdots,j+1)}\right)\right]}{\sqrt{\left[\sum_{i=0}^{M-1}\left(I(i,j)-\overline{I(\cdots,j)}\right)^2\right]\left[\sum_{i=0}^{M-1}\left(I(i,j+1)-\overline{I(\cdots,j+1)}\right)^2\right]}}\right)}{N-1} \tag{4.8}$$

On the other hand, rows of the 2D representation of the data also carry distinguishable information for classification since they contain the changes in the duration of one period of the data. These periodicity fluctuations result in some inconsistent shifting effects that can only be analyzed with the relationship between neighbor columns of the horizontal image. Equation (4.9) gives the mean of the cross-correlation coefficients among neighbor rows within the images where *N* and *M* denote the number of columns and rows respectively.

$$r_{row} = \frac{\sum_{i=0}^{M-2}\left(\frac{\sum_{j=0}^{N-1}\left[\left(I(i,j)-\overline{I(i,\cdots)}\right)\left(I(i+1,j)-\overline{I(i+1,\cdots)}\right)\right]}{\sqrt{\left[\sum_{j=0}^{N-1}\left(I(i,j)-\overline{I(i,\cdots)}\right)^2\right]\left[\sum_{j=0}^{N-1}\left(I(i+1,j)-\overline{I(i+1,\cdots)}\right)^2\right]}}\right)}{M-1} \tag{4.9}$$

Row correlation that calculated for the horizontal image has close similarity with autocorrelation value $R_{xx}(N)$ for 1D signal where N is the period of 1D signal, which is also the width of the 2D grayscale image upon the wavelet decomposition is performed. This naturally corresponds to an autoregressive model, AR-1 with a correlation coefficient, ρ, and a fixed time-lag of N:

$$x[n] = \rho_N x[n-N] + \varepsilon[n] \tag{4.10}$$

where $\varepsilon[n]$ is the model error.

Column correlation that calculated for the vertical has close similarity with autocorrelation value $R_{xx}(1)$ for the one-dimensional signal. This time, the model corresponds to the simple AR-1 with a different correlation coefficient and a simple time-lag of 1:

$$x[n] = \rho_1 x[n-1] + \varepsilon[n] \tag{4.11}$$

where $\varepsilon[n]$ is the model error.

The reason behind calculating row and column correlations of the horizontal and vertical wavelet components of the 2D image, instead of calculating AR(1) parameters directly from 1D signal, is the strengthened information about $R_{xx}(N)$ and $R_{xx}(1)$ by the wavelet decomposition that also corresponds to horizontal and vertical textures in the 2D image representation of the 1D signal. Horizontal textures are more distinct in horizontal component than the original 2D image representation due to the filtering effects of vertical textures. The same case is also valid for vertical textures in vertical component because of filtering effects of horizontal textures.

The energy image is expected to lack texture information, however experiments show that single level wavelet decomposition is insufficient for strict extraction of the detail information from the 2D representation. Thus, energy image has still some detail information, which may help for the analysis of the texture in parallel with the classification of the motor fault type. In order to obtain the necessary information contained by the energy image, column correlation is also

calculated for energy image, instead of applying second level wavelet decomposition.

4.4. Local Binary Pattern Based Feature Extraction from 2D Grayscale Image Representation of the Data

The local binary pattern operator can be defined as an image operator which converts an image into an array or image having integer labels which describes small-scale appearance of the image. These integer labels or their statistical properties, most commonly the histograms, are used for further analysis and feature extraction (Mäenpää, 2003; Pietikäinen et al., 2011).

The basic local binary pattern texture analysis operator, which is introduced by Ojala et al., is a grayscale invariant texture measure (Ojala et al., 1996). The local binary pattern (LBP) operator labels each pixel by tresholding its *p* neighbors' pixel value with the center pixel's value and converts the result into a pattern code by the equation:

$$LBP(\mathrm{x}_c, \mathrm{y}_c) = \sum_{p=0}^{p-1} s(\mathrm{g}_p - \mathrm{g}_c) 2^p, \qquad where \qquad s(\mathrm{x}) = \begin{cases} 1 & x \geq 0 \\ 0 & x < 0 \end{cases}, \tag{4.12}$$

g_c denotes the gray value of the center pixel (x_c,y_c) and g_p denotes the gray values of p equally spaced pixels on the circumference of a circle with radius R as shown in Figure 4.9.

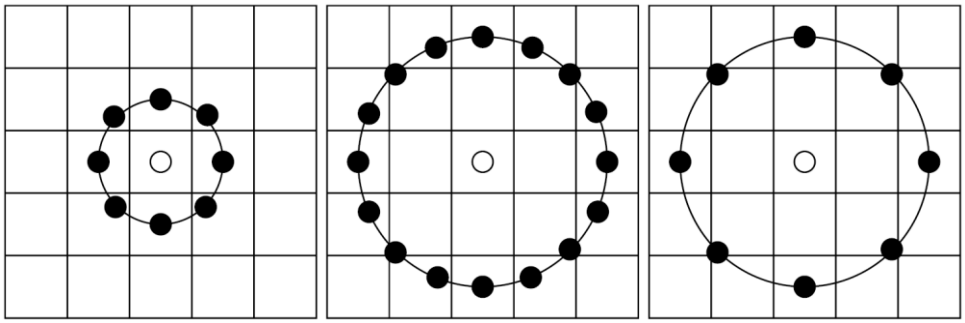

Figure 4.9. The circular (8, 1), (16, 2) and (8, 2) neighborhoods of LBP operator

LBP is a highly discriminate operator which records the occurrences of various patterns in the neighborhood of each pixel in a histogram. Since the signed difference g_p-g_c is not affected by changes in mean luminance, a grayscale shift does not affect the LBP code of an image. Therefore, LBP operator is a rotation invariant operator against any monotonic transformation of the grayscale values of the images (Shahriar et al., 2013).

The original version of the local binary operator uses a 3x3 pixel block of an image which can be shown on the left of the Figure 4.9. The calculation of a pattern code with basic LBP operator on a 3x3 pixel block of an image is illustrated by an example given in Figure 4.10.

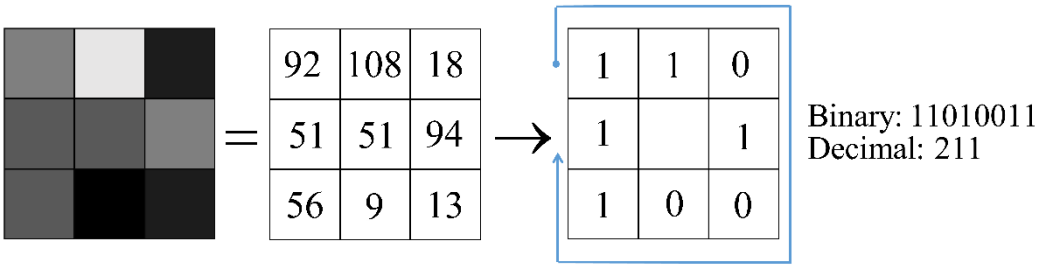

Figure 4.10. Pattern code generation by the basic LBP operator

After calculating the LBP code for each pixel (x_c, y_c), the original input image of size MxN is represented by an LBP histogram H by the equations below:

$$H(\tau) = \sum_{y_c=1}^{M-1} \sum_{x_c=1}^{N-1} f\left(LBP_{p,R}(x_c, y_c), \tau\right) \quad where \quad \tau \in [0, \mathrm{K}], \tag{4.13}$$

and;

$$f(\mathrm{a}, \tau) = \begin{cases} 1 & a = \tau \\ 0 & else \end{cases} \tag{4.14}$$

where K is the maximum value of the LBP code. Since for basic LBP operator, the p neighborhood is 8, τ will have 2^8 different labels. Therefore, 256 histogram bins $H(\tau)$ will be acquired from the images, which can be used as texture descriptor.

LBP technique can be applied to the square shaped grayscale images that are created from the current, vibration and acoustic data. In Figure 4.11, the original grayscale images and their corresponding LBP images and normalized histograms are depicted. By inspection of these images and histogram bins, differences related to motor faults can be seen.

In this thesis, LBP related features are extracted from normalized LBP histograms. Since the sizes of the grayscale images change due to the sampling frequency and the loading conditions of the test motors, normalized histograms of length 256 are used as feature sources. Three of four fundamental statistical parameters, standard deviation, skewness and kurtosis of the histograms are chosen as the first three features. Since the histograms are normalized, mean parameter become useless in feature selection. In order to observe the repeating patterns of the histograms, it is reasonable to use autocorrelation function. Afterwards, autocorrelation of the data with itself by neighborhood shifts of 1 to 5 are chosen as the remaining five features. By this manner, 8-dimensional feature sets are extracted from only using the acquired LBP histograms.

Classification performances of features acquired from current, vibration and acoustic data are given in results section. When compared to other methods proposed in this thesis, LBP based feature extraction requires minimal computational cost.

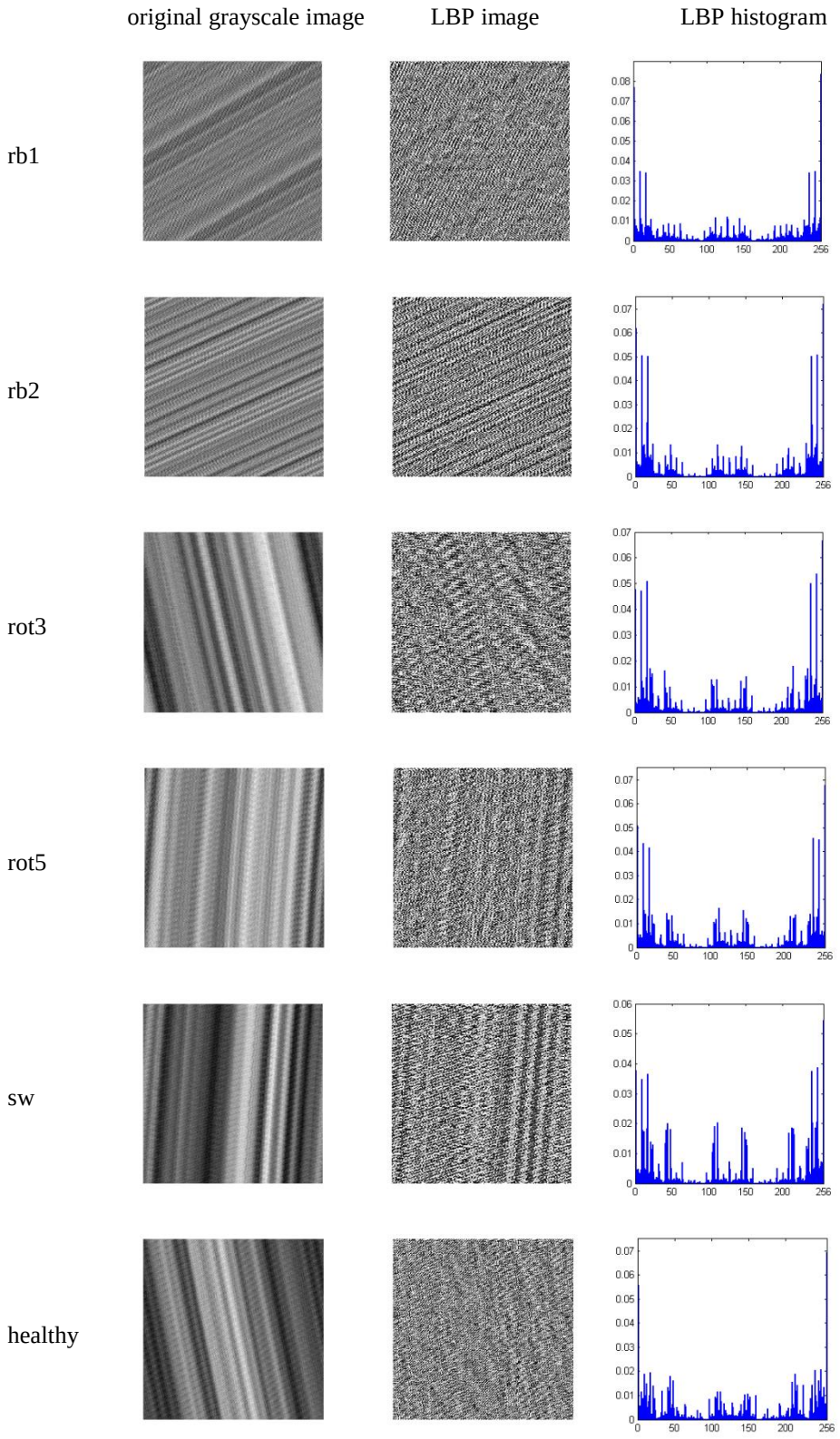

Figure 4.11. Original grayscale images, LBP images and LBP histograms of vibration data of test motors operating under 4.7 Amperes load

5. FAULT CLASSIFICATION METHODS

In this thesis, different classification algorithms are applied to the feature sets obtained by the proposed methods explained in section 4 from supply current, vibration and acoustic data to discriminate and classify the fault types of induction motors. Fault classification is performed using three different well-known classifiers namely linear discriminant classifier (LDC), quadratic discriminant classifier (QDC) and Fisher's linear discriminant analysis (LDA). Classification performances of each classifier are compared in order to decide which one is more sensible for the selected feature sets.

5.1. Fault Classification with Linear and Quadratic Bayesian Classifiers

Linear and quadratic classifiers are named due to the type of discriminant functions they use. Any set of linear functions $g_i : \Re^n \to \Re, \quad i = 1, 2, \cdots, N$,

$$g_i(\mathbf{x}) = \mathrm{w}_{i0} + \boldsymbol{w}_i^T \boldsymbol{x}, \qquad x, w_i \in \Re^n, \quad w_{i0} \in \Re \tag{5.1}$$

can be thought as a linear classifier. Linear classifier is derived as the minimum-error Bayes classifier for normally distributed classes with equal covariance matrices and this model is called linear discriminant classifier. It is reasonably robust classifier and works well even with the classes which do not have normal distributions (Kuncheva, 2004).

Both of the classifiers, LDC and QDC inherit from the famous Bayes classifier that works according to a decision rule to minimize the probability of classification error and come up with the a-posteriori probability maximization:

$$p(\mathrm{x}|c_i)\, p(\mathrm{c}_i) > p(\mathrm{x}|c_j)\, p(\mathrm{c}_j) \qquad j = 1, 2, \cdots, N; \qquad j \neq i \tag{5.2}$$

where a feature vector x is assigned to class c_i among the classes $c_1, c_2, \ldots, c_N$ if the a-posteriori error statement is satisfied (Duda et al., 2012). Both LDC and QDC

are special cases of this selection creation under the assumption of Gaussian probability density functions (Van Der Heijden et al., 2005). In LDC, the covariances of each class are assumed to be exactly the same, so the comparison simplifies to the nearest neighbor selection rule:

$$\|\boldsymbol{x}-\boldsymbol{\mu}_i\| > \|\boldsymbol{x}-\boldsymbol{\mu}_j\| \qquad j=1,2,\cdots,N; \qquad j\neq i \tag{5.3}$$

The quadratic case arises when the covariance matrices ($\mathbf{C}_i$) of each class are treated separately under Gaussian distribution assumption:

$$(\mathbf{x}-\boldsymbol{\mu}_i)^T \boldsymbol{C}_i^{-1}(\mathbf{x}-\boldsymbol{\mu}_i) > (\mathbf{x}-\boldsymbol{\mu}_j)^T \boldsymbol{C}_j^{-1}(\mathbf{x}-\boldsymbol{\mu}_j) \qquad j=1,2,\cdots,N; \qquad j\neq i \tag{5.4}$$

5.2. Fault Classification with Fisher's Linear Discriminant Analysis

This classifier depends on the Fisher's linear discriminant analysis (LDA), which was developed in 1936 (Fisher, 1936). This classifier is also a linear classifier, but unlike LDC, it utilizes covariance structures of both within-class and between-class relations by projecting the features onto a best separation direction. This best linear separation is equivalent to minimizing the distance between members of the same class while maximizing the distance to members of the remaining (other) classes. To find a transformation for the regarding subspace, the following criterion function is maximized:

$$J(\mathbf{W}) = \frac{\left|\mathbf{W}^T \mathbf{S}_B \mathbf{W}\right|}{\left|\mathbf{W}^T \mathbf{S}_W \mathbf{W}\right|} \tag{5.5}$$

where W is the transformation matrix, and S_B and S_W denote the between-class and within-class scatter matrices, respectively (Welling, 2005). Once transformation is constructed, data vectors are applied to this transform by means of vector-matrix multiplication, and then the nearest mean decision rule is used for classification in the transformed vector space. In multi-class case, the analysis used in the derivation

of the Fisher discriminant can be extended to find a subspace which appears to contain all of the class variability (Rao, 1948).

5.3. Fault Classification with Self Organizing Maps

Self-organizing map (SOM) is a well-known method to organize the input feature vectors. Since SOM algorithm is a vector quantization variant, the class boundaries should be adjusted well in order to improve the quality of the quantization. The supervised Learning Vector Quantization (LVQ) algorithm provides a suitable method to adjust boundaries. Although there are separate algorithms in the literature about LVQ, the LVQ3 algorithm preferred in this thesis (Kohonen, 1990).

SOM provides a powerful method based on Hebbian type neural network for the classification problems. The main consequence of the SOM is the possibility of tracing the similarities and the discrepancies of the input data. SOM projects the input data vector $\Lambda \in \mathbb{R}^n$ which is taken from a sample space of size *p* to the *m* many codebook vectors of $M \in \mathbb{R}^n$ which organized in planar fashion where $p \gg m$. The result after training SOM is a lattice of neurons representing the possible clusters.

In the training phase, SOM is organized in an unsupervised manner according to the equation (5.6):

$$M_i(\mathrm{k}) = \mathrm{M}_i(\mathrm{k}-1) + (\alpha(\mathrm{k}) \cdot \beta(\mathrm{i},\mathrm{c},\mathrm{k}) \cdot [\Lambda(\mathrm{k}) - \mathrm{M}_i(\mathrm{k}-1)] \quad \forall i \quad 1 \le i \le m \qquad (5.6)$$

where $\alpha(k)$ is the learning rate and $\beta(i,c,k)$ is the neighborhood parameter which change in the adaptation phase. The index of the best matching neuron, which is denoted as *c*, is a parameter which depends on:

$$c = \arg\min_i \left\| \Lambda(\mathrm{k}) - \mathrm{M}_i(\mathrm{k}) \right\|. \qquad (5.7)$$

After training phase, the codebook vectors organized in planar lattice structure and for each input vector, the closest codebook vectors represent the possible cluster. A supervised method Learning Vector Quantization 3 (LVQ3) algorithm is used in order to describe the classification regions, and the region of clusters (Kohonen, 1995). This algorithm can be expressed as:

$$M_i(\mathrm{k}+1) = \mathrm{M}_i(\mathrm{k}) - (\xi(\mathrm{k}) \cdot [\Lambda(\mathrm{k}) - \mathrm{M}_i(\mathrm{k})]) \tag{5.8}$$

$$M_j(\mathrm{k}+1) = \mathrm{M}_j(\mathrm{k}) - (\xi(\mathrm{k}) \cdot [\Lambda(\mathrm{k}) - \mathrm{M}_j(\mathrm{k})]) \tag{5.9}$$

where M_i and M_j are the two closest codebook vectors for $\Lambda(\mathrm{k})$, and both $\Lambda(\mathrm{k})$ and M_j belongs to the same class however M_i is not. Also it is necessary that M_i, M_j and $\Lambda(\mathrm{k})$ have to be in the window as:

$$\min\left(\frac{d_1}{d_2}, \frac{d_2}{d_1}\right) > s \quad \textit{where} \quad \frac{1 - \textit{window}}{1 + \textit{window}} \tag{5.10}$$

where d_1 and d_2 are the distances between the closest codebook vector M_i and the input data $\Lambda(\mathrm{k})$ and second closest codebook vector M_j and $\Lambda(\mathrm{k})$ respectively.

In the algorithm if M_i and M_j are in the same class than the adaptation scheme will be as:

$$M_i(\mathrm{k}+1) = \mathrm{M}_i(\mathrm{k}) - (\eta \cdot \xi(\mathrm{k}) \cdot [\Lambda(\mathrm{k}) - \mathrm{M}_i(\mathrm{k})]) \tag{5.11}$$

$$M_j(\mathrm{k}+1) = \mathrm{M}_j(\mathrm{k}) - (\eta \cdot \xi(\mathrm{k}) \cdot [\Lambda(\mathrm{k}) - \mathrm{M}_j(\mathrm{k})]) \tag{5.12}$$

where η and $\xi(\mathrm{k})$ are learning rate parameters.

6. RESULTS

6.1. Classification Results with Features Obtained by Calculating Wavelet Packet Decomposition Coefficients of the Current Data

Stator current data of induction motors couple with the adjustable speed drive is acquired at 20 kHz sampling rate at three different speed references and load conditions with a duration of forty seconds, as mentioned in Sections 3 and 4, result in data files of length 800,000 samples. By applying 11^{th} level of WPD to the elements of the stator current data by a sliding window of length 400,000 with a slide amount of 10,000 samples, the wavelet packet coefficients related to three specific nodes covering the frequency region 43.92 to 58.56 Hz are calculated at 40 instances. By calculating the four fundamental statistical parameters (mean, standard deviation, skewness and kurtosis) of the coefficients at each of the three nodes, 12-dimensional 40 feature vectors are obtained. Fault classification is performed by using three different well known classifiers, linear discriminant classifier (LDC), quadratic discriminant classifier (QDC) and Fisher's linear discriminant analysis (LDA). Besides, same procedure is performed by changing the size of the sliding window length to 20,000 in order to observe the effect of selected wavelet filter type on classification process. Four different members of wavelet families, Haar, Daubechies2 (db2), Daubechies8 (db8) and Daubechies32 (db32) are selected wavelet filters in this thesis that provides to observe the effect of filter length in WPD at higher decomposition levels.

The first approach is to classify fault types under different load conditions at each selected speed reference frequencies. In this thesis, feature vectors are obtained from six 2.2 kW induction motors running at the same speed via the output of the adjustable speed drive at three different loading conditions which cause 4.1, 4.7 and 5 Amperes of stator currents. These three different load conditions were considered separately resulting three different sets of data. Test motors are classified with the mentioned classifiers at each load level. Feature vectors are obtained by selecting the wavelet type in WPD, therefore four different wavelet types are tested separately. Classifier performances are evaluated by applying n-

fold cross validation (leave-one-out method) so that the overall data set is tested. Classification results for this approach is given in Tables 6.1 to 6.3, which shows the classification error percentages under speed reference frequencies of 35, 40 and 50 Hz in order.

Table 6.1. % of classification errors for motors run with speed reference of 50 Hz

		Selected wavelet type			
Selected Classifier	Load Level (A)	Haar	db2	db8	db32
LDA	4.1	0.42	0.00	0.83	6.67
	4.7	0.00	0.00	1.67	0.00
	5.0	0.00	0.00	0.00	0.00
QDC	4.1	0.00	0.00	0.00	5.42
	4.7	0.00	0.00	0.00	0.00
	5.0	0.00	0.00	0.00	0.00
LDC	4.1	0.00	0.00	0.00	0.00
	4.7	0.00	0.00	0.00	0.00
	5.0	0.00	0.00	0.00	0.00

Table 6.2. % of classification errors for motors run with speed reference of 40 Hz

		Selected wavelet type			
Selected Classifier	Load Level (A)	Haar	db2	db8	db32
LDA	4.1	0.00	0.00	0.83	5.42
	4.7	5.83	4.58	7.92	3.75
	5.0	0.42	0.00	0.42	0.00
QDC	4.1	0.00	0.00	0.42	2.50
	4.7	0.00	0.00	0.83	3.33
	5.0	0.00	0.00	0.00	0.00
LDC	4.1	0.00	0.00	0.42	1.25
	4.7	0.00	0.00	0.42	2.50
	5.0	0.00	0.00	0.00	0.00

Table 6.3. % of classification errors for motors run with speed reference of 35 Hz

		Selected wavelet type			
Selected Classifier	Load Level (A)	Haar	db2	db8	db32
LDA	4.1	2.92	0.83	1.67	1.25
	4.7	0.83	0.00	0.00	1.25
	5.0	0.00	0.00	0.00	2.08
QDC	4.1	0.00	0.00	0.00	0.42
	4.7	0.00	0.00	0.42	0.83
	5.0	0.00	0.00	0.00	0.00
LDC	4.1	0.00	0.42	1.67	0.00
	4.7	0.00	0.00	0.00	0.42
	5.0	0.00	0.00	0.00	0.00

When overall recognition accuracies given it Tables 6.1 to 6.3, for all load levels and filter types, QDC performs better than both LDA and LDC. QDC is indeed superior to LDA overall, although in some cases, Fisher's LDA classification success rates are comparable with ones obtained from QDC. The deliberate change of load levels and speed reference frequencies provided us with observations regarding the feature vector position on the multi-dimensional feature space. It is expected that features obtained from the same class motor under the same load and speed reference frequency should constitute a compact cluster on the multi-dimensional feature space. On the other hand, depending on the type of classifiers, other features from another motor should form a different cluster which could be separated from the previous one using hyper-planes or hyper-curves. The superior performance of QDC over other classifiers used here reveals that the proposed feature vectors belonging to different motors with different faults can be best distinguished with quadratic hyper-curves. In order to illustrate this situation for the proposed feature set, in Figures 6.1 to 6.3, the examples of mentioned clusters with selected features are presented as 3D scatter plots, using selected wavelet filter type of db2, for load and speed reference frequency conditions of 4.1 A at 35 Hz, 4.7 A at 40 Hz, and 5 A at 50 Hz, respectively. It can be noted that the amount of load and speed reference frequency seem to have no significant effect on the recognition rate as long as the proper classifier is used. To sum up, the argument

is that the proposed set of feature vector elements, which are the statistical parameters extracted from WPD coefficients constitute a reasonable feature set with satisfactory classification results.

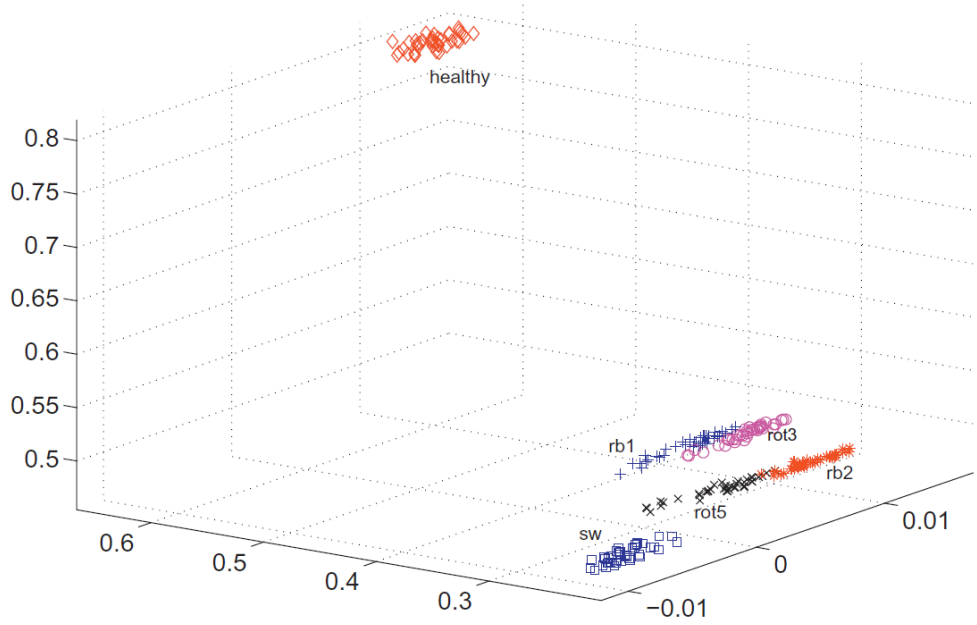

Figure 6.1. Feature clusters at 4.1 A at 35 Hz

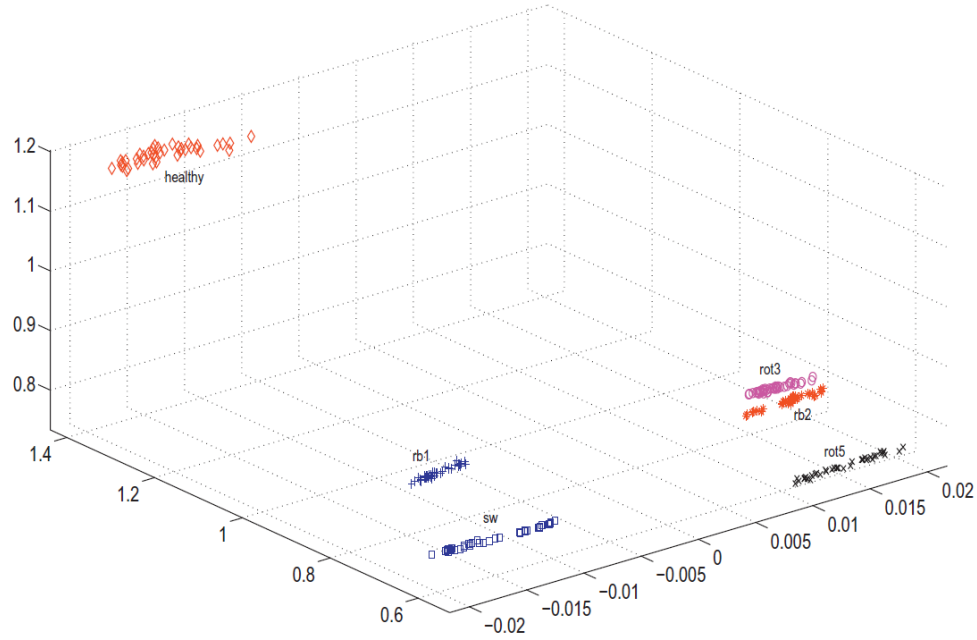

Figure 6.2. Feature clusters at 4.1 A at 40 Hz

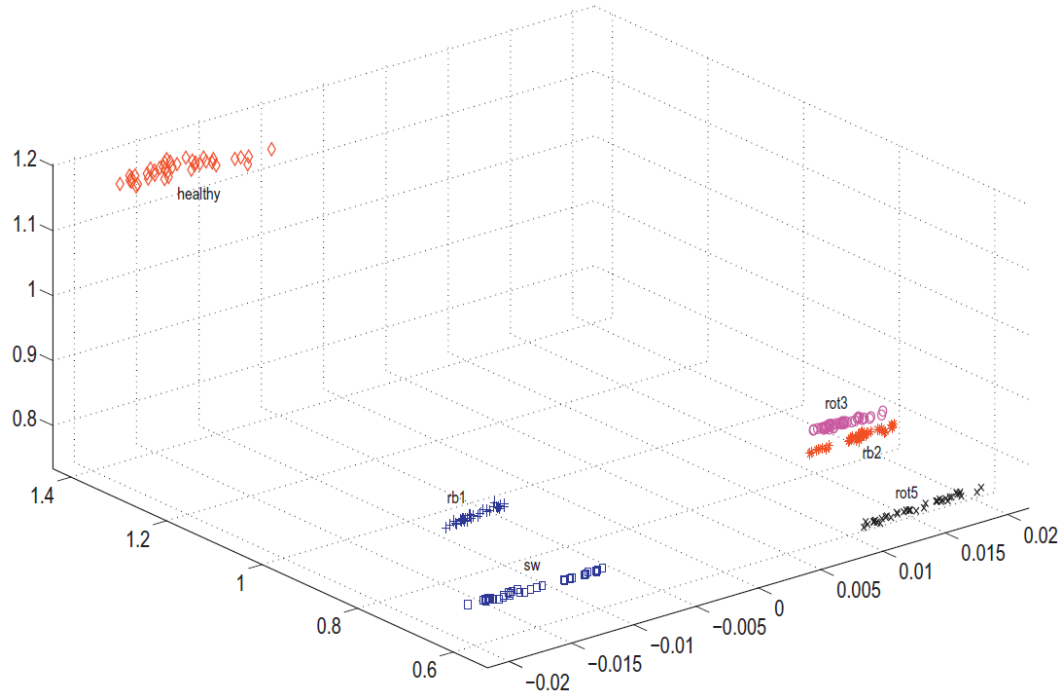

Figure 6.3. Feature clusters at 5.0 A at 50 Hz

The detection and classification of induction motor faults by motor current signature analysis, requires the detailed analysis of very narrow bands in the frequency spectrum regardless of adjustable speed drive supplied motor or 3-phase direct line supplied motor. So, this becomes a necessity that the current data must be obtained at high sampling rates therefore a good frequency resolution is reached in considered narrow bands and the method that is used in extracting features from these bands must be applied carefully. If the data length is not sufficiently long, WPD yields very short data segments and low frequency resolution at nodes in high decomposition levels due to the successive down sampling. In such a case, convolution of selected wavelet filter with data in a node to obtain decomposition samples may become meaningless if the selected filter size is almost equal or longer than the data length in a node. For example in literature, seven level WPD is applied to motor current data of 150,000 samples result in 31 samples at nodes corresponding to frequency bands of interest (Teotrakool et al., 2009). The selected filter type has a size of 24 which is comparable to the data length at nodes considered resulting arguable classification success rate. Also in this thesis, regardless of the load condition and speed reference frequency, all classifiers

performed well except the case when the selected filter type is db32 which has a filter length of 64. This outcome of short data size was also tested by applying 11^{th} level of WPD to motor stator current data size of 20,000 and the classification results are presented in Table 6.4. Poor classification results were observed as the selected wavelet filter size increases.

Table 6.4. % of classification errors for motors run with speed reference of 35 Hz (20,000 samples in WPD)

		Selected wavelet type			
Selected Classifier	Load Level (A)	Haar	db2	db8	db32
LDA	4.1	0.00	4.58	2.50	8.33
	4.7	2.92	9.58	14.17	14.17
	5.0	0.00	3.75	4.58	4.17
QDC	4.1	0.00	0.83	0.42	8.33
	4.7	0.83	3.33	11.25	11.25
	5.0	0.00	0.42	3.33	2.50
LDC	4.1	4.58	12.50	12.50	8.75
	4.7	12.08	23.75	19.17	22.92
	5.0	2.08	4.17	4.58	15.42

Performing the classification at a fixed load condition is not general enough to test the efficiency of the proposed features for arbitrary and practical engineering applications. Hence another approach is adopted where the data are explicated regardless of the load. In this manner, combined feature vector data of 120 sets for each motor are used in the classification process, corresponding to all three load levels. Percent classification errors regardless of the load condition at 40 Hz are given in Table 6.5. Again, the performance of QDC is superior to LDC and LDA. In this case also, as the selected wavelet filter size increases, the recognition rate diminishes. However, the classification accuracy obtained by using QDC is very high and it may easily be observed that proposed feature vector elements are capable of perfectly representing different motor faults in an ASD-motor combination once a proper classifier is selected. The successful classification

results are also showed in the form of a confusion matrix for QDC at 40 Hz speed reference and using wavelet filter type of db8 in Table 6.6.

Table 6.5. % of classification errors for motors run with speed reference of 35 Hz regardless of load

		Selected wavelet type			
Speed Reference	Selected Classifier	Haar	db2	db8	db32
35 Hz	LDA	33.33	23.20	22.92	32.64
	QDC	0.28	0.00	3.75	9.03
	LDC	30.00	20.00	18.75	30.83
40 Hz	LDA	16.94	22.36	22.56	33.06
	QDC	0.00	0.00	2.78	3.47
	LDC	12.92	17.91	19.17	32.78
50 Hz	LDA	10.69	13.75	17.64	23.47
	QDC	0.00	0.00	1.11	3.47
	LDC	11.11	11.67	15.56	19.31

Table 6.6. Confusion matrix for QDC with db8 filter regardless of load at speed reference of 40 Hz

	Predicted					
	rb1	rb2	rot3	rot5	sw	healthy
rb1	120	0	0	0	0	0
rb2	0	118	2	0	0	0
rot3	0	7	113	0	5	0
rot5	0	0	0	119	1	0
sw	0	0	10	0	110	0
healty	0	0	0	0	0	120

It is obvious from the results of this work that any fault perturbs the supply side current of ASD-motor combination in terms of significant changes in the statistical parameters of WPD coefficients. Clearly, the leakage of the injected energy into harmonic components other than the fundamental increases with the

existence of a motor fault and the proposed feature vector elements are good indicators of this change in energy.

6.2. Classification Results with Features Obtained from Acoustic Data Using Self-Organizing Maps

In order to classify motor faults, with SOM, a combined feature vector set is used. 40 combined features obtained from both cross correlations of acoustic data recorded by different microphones and features obtained from the wavelet decomposition of the 2D images constructed from 1D sound data of each microphone are added into the combined feature set and listed in Table 6.7. Also, the flow diagram of the entire feature extraction and classification process is given below in Figure 6.4.

Table 6.7. Combined feature set for acoustic based and classification process

Cross-Correlation Features		Wavelet Decomposition Features (from the images constructed from the acoustic data recorded by microphones 1 to 5)
#1: $r_{\chi_1\chi_2}$	#6: $r_{\chi_2\chi_4}$	#11, #17, #23, #29, #35: RMS energy of vertical images
#2: $r_{\chi_1\chi_3}$	#7: $r_{\chi_2\chi_5}$	#12, #18, #24, #30, #36: RMS energy of diagonal images
#3: $r_{\chi_1\chi_4}$	#8: $r_{\chi_3\chi_4}$	#13, #19, #25, #31, #37: Column correlation of vertical images
#4: $r_{\chi_1\chi_5}$	#9: $r_{\chi_3\chi_5}$	#14, #20, #26, #32, #38: Column correlation of diagonal images
#5: $r_{\chi_2\chi_3}$	#10: $r_{\chi_4\chi_5}$	#15, #21, #27, #33, #39: Row correlation of horizontal images
		#16, #22, #28, #34, #40: Column correlation of energy images

In order to train a 5x10 dimensional SOM, the feature vectors obtained from two different experiment sets (Exp1 and Exp3) are used. Prior to training, the input vectors are normalized. After training phase, the resultant map in Figure 6.5 has been obtained. Naturally, the SOM results depends on the nature of the feature vectors. In this work the vectors are composed of both cross correlation values of time domain data and the image-related correlations as explained in Section 4.

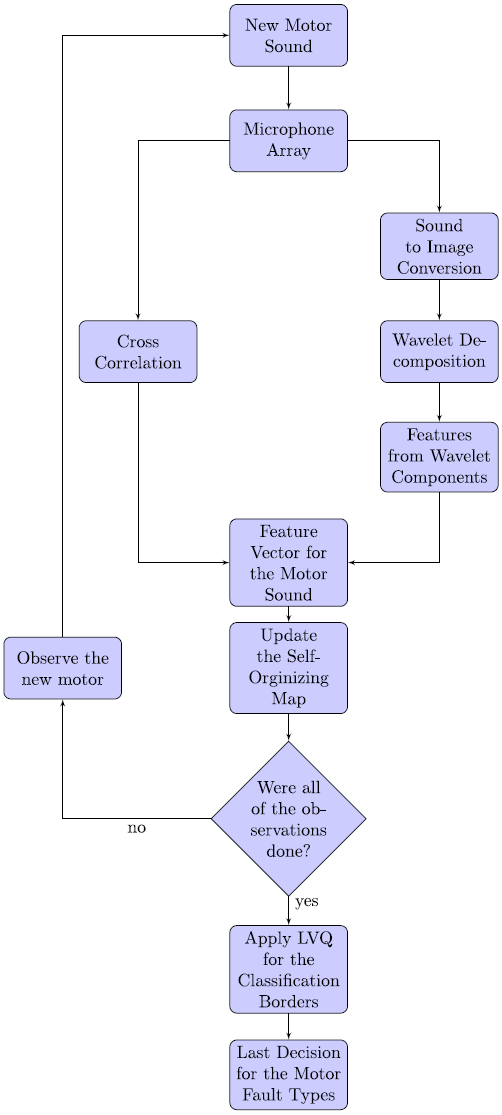

Figure 6.4. Flow diagram of the entire feature extraction and classification process of acoustic data with SOM

The motor number labels, which can be seen on the map, are the corresponding localizations of the training motor data on the map. The vicinity in two-dimensional map shows the possible close relationship of the input feature vectors. In other words, if two feature vectors from two different experiments are mapped to neurons which are close to each other in the lattice, it is possible to deduce that there is somehow a resemblance between those motors. Conversely, the increase in the space between the neurons indicates the differences of the features obtained from the motors.

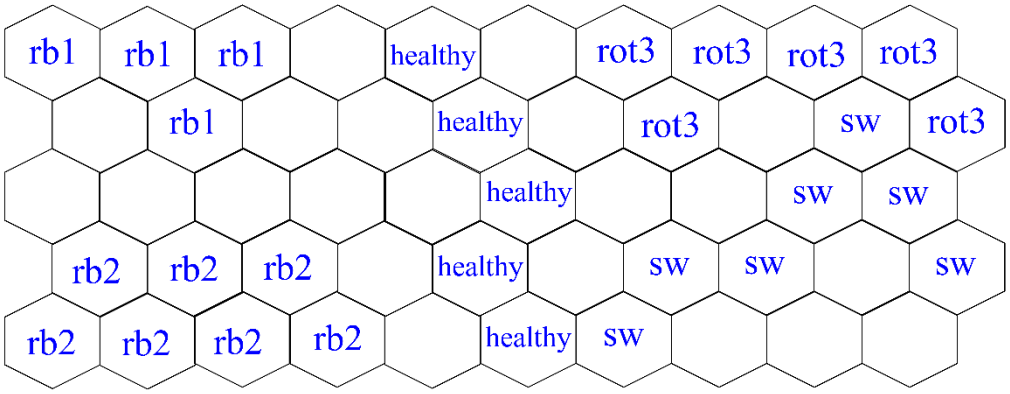

Figure 6.5. 5x10 Dimensional SOM map trained with Exp1 and Exp3 dataset

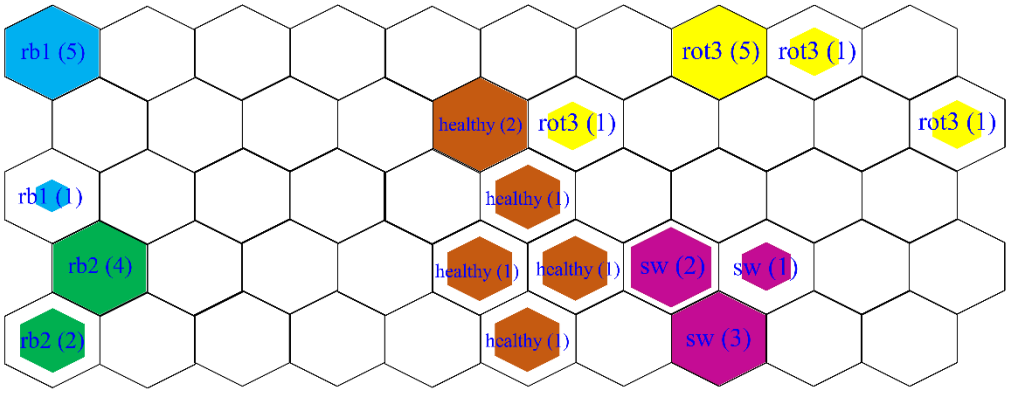

Figure 6.6. Localization of test data from Experiment 2 on 5x10 Dimensional SOM map

By inspecting Figure 6.6, rb1 and rb2 data have been localized at the left of the healthy motor and the other faults are settled at the right of the healthy one. It is not surprising that rb1 and rb2 faults have some close relationship with each other since being ball bearing related problems and the SOM map has a consistent result with this relationship. In order to test the results, the experiment set Exp2 data are directly applied to the trained map and the following results have been obtained. Clearly, the test data localization is highly consistent with the trained data at a first glance. In Figure 6.6, the number in parentheses designates the number of hits for the relevant motor.

Table 6.8 demonstrates the classification performance without applying LVQ algorithm. After applying LVQ3 algorithm, the results show the improvement in the classification performance as shown in Table 6.9.

Table 6.8. Confusion matrix and correct classification results of test data without applying LVQ algorithm

	Predicted					
	healthy	rb1	rb2	rot3	sw	classification %
healthy	6	0	0	0	0	100
rb1	0	6	0	0	0	100
rb2	0	0	6	0	0	100
rot3	1	0	0	5	0	83
sw	0	0	0	0	6	100

Table 6.9. Confusion matrix and correct classification results of test data after applying LVQ algorithm

	Predicted					
	healthy	rb1	rb2	rot3	sw	classification %
healthy	6	0	0	0	0	100
rb1	0	6	0	0	0	100
rb2	0	0	6	0	0	100
rot3	0	0	0	6	0	100
sw	0	0	0	0	6	100

6.3. Comparative Classification Results of Current, Vibration and Acoustic Data with Linear and Quadratic Bayesian Classifiers

In this thesis, different classification approaches are proposed for current, vibration and acoustic data. WPD of stator current data works well with the current data obtained from the motors driven with adjustable speed drive. But in many

applications, the use of driving of motors directly with AC network is very common. In order to make a comparative classification between current, vibration and acoustic monitoring, these three different data are collected with three sets of experiments. Vibration and current data are sampled with 20 kHz and collected simultaneously with NI-6251 data acquisition card. But it was impossible to collect sound data recorded with 5 microphones simultaneously. With another PC, acoustic data are tried to be collected at a sampling rate of 44.1 kHz at the same time of the collection of vibration and current but it is sure that pure synchronization of the processes are not possible. It is worth to note that some time delays exist between these two parallel data acquisition processes.

Cross-correlation based features worked well for acoustic based classification with five microphones which make simultaneous recording but these kind of features are useless for current and vibration. In order to make a fair comparison, features obtained by converting 1D data to 2D grayscale images are used. Images are constructed as square shaped whose width is equal to the number of samples of a period of a signal which is calculated by finding the autocorrelation of the signal. According to the size of the collected data samples, number of created grayscale images changes due to the sampling frequencies. For this reason, from each trial of the experiments, four grayscale images are constructed for current and vibration data while only one grayscale image can be constructed for acoustic data for recordings of a single microphone. Since the classification performances are compared, this difference does not affect the classification process. Also for acoustic data, recordings of separate microphones are converted to grayscale images separately and for each trail, features are obtained from each five images are added separately to the feature set. After applying single level of 2D DWT to all images, features are obtained using some properties of the sub-band images as described in section 4. These six features are, RMS energy of vertical images, RMS energy of diagonal images, column correlation of vertical images, column correlation of diagonal images, row correlation of horizontal images, and column correlation of energy images. Classification performance of LDC and QDC, regardless of loading condition using six features can be seen in Table 6.10.

Table 6.10. Comparative % of classification errors for different types of data of motors regardless of load

	selected classifier	
selected data type	LDC	QDC
current data	43.75	21.99
acoustic data	24.07	14.44
vibration data	6.94	1.85

Results are quite well for acoustic and vibration data even only 6 features are used for classification. But when compared to WPD based classification, this method provides very poor classification performance for current data. Also QDC is superior to LDC for each data type. A detailed look to classification errors can be seen by the confusion matrices given for acoustic and vibration data using QDC in Tables 6.11 and 6.12.

Table 6.11. Confusion matrix for QDC for acoustic data regardless of load

	Predicted					
	rb1	rb2	rot3	rot5	sw	healthy
rb1	84	6	0	0	0	0
rb2	0	79	11	0	0	0
rot3	0	0	78	8	0	4
rot5	0	0	12	57	18	3
sw	0	0	1	10	79	0
healty	0	0	3	2	0	85

Table 6.12. Confusion matrix for QDC for vibration data regardless of load

	Predicted					
	rb1	rb2	rot3	rot5	sw	healthy
rb1	72	0	0	0	0	0
rb2	0	72	0	0	0	0
rot3	0	0	68	0	4	0
rot5	0	0	1	70	1	0
sw	0	0	0	1	71	0
healty	0	0	1	0	0	71

From the confusion matrices, it can be stated that vibration data is more sensitive for differentiating bearing faults. It can be also seen by scatter plot of arbitrarily selected 3 features over 6 in Figure 6.7.

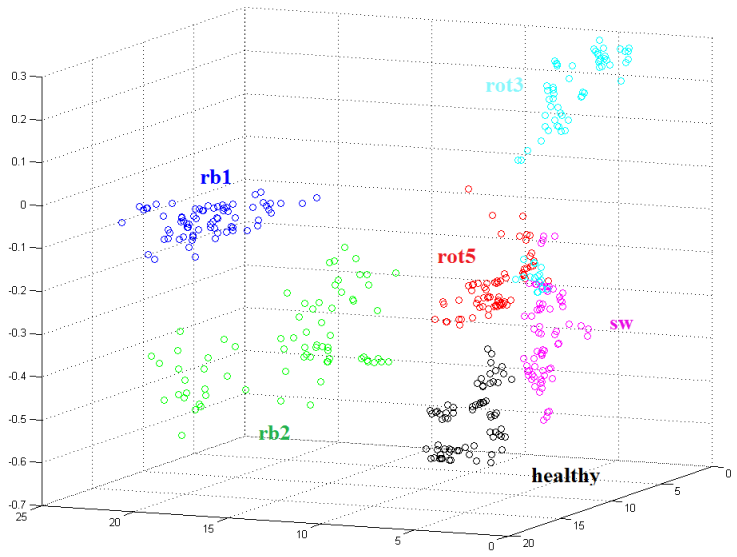

Figure 6.7. Feature clusters of vibration based features regardless of load

As it can be seen in Figure 6.7, feature clusters of bearing faults are separated from other fault clusters and they lie in the same direction but in separate clusters. Features of broken rotor bar faults of 3 and 5 broken bar problems' clusters are close to each other, is also an expected result.

Acoustic data were obtained using 5 different microphones simultaneously. When the features related to each microphone are lumped together, which results in 30-dimensonal feature vector instead of 6. This new group of features provide better results for acoustic based fault classification.

Table 6.13. Comparative % of classification errors for acoustic data related features of motors regardless of load

	selected classifier	
selected feature set	LDC	QDC
6 features	24.07	14.44
30 features	1.85	6.48

6.4. Classification Results with Features Obtained by LBP Histograms

The 8-dimensional feature vectors which are extracted by only using the properties of the acquired LBP histograms from the square shaped grayscale images constructed from current, vibration and acoustic data are used for classification of the motor faults.

Classification performances of data types are compared by using three different well known classifiers, linear discriminant classifier (LDC), quadratic discriminant classifier (QDC) and Fisher's linear discriminant analysis (LDA). Vibration data gives the best performance, approximately 95% correct classification with only 8 features with QDC. Also as it is seen from the results, current data is not sensible for this type of feature extraction technique since it shows more stationary characteristic compared to vibration and acoustic data.

Table 6.14. % of classification errors for LBP histograms based fault classification of motors regardless of load

	selected classifier		
	LDA	QDC	LDC
Current Data	45.14	27.13	46.06
Vibration Data	15.74	5.32	16.20
Acoustic Data	22.41	6.48	18.89

7. CONCLUSION

Induction motors are the most widely used electrical machines in industry due to their simple construction, cost effectiveness and easy maintenance. In this thesis, fault classification of induction motors are realized with the current, vibration and acoustic data acquired by various experiments in laboratory environment. In order not to interrupt the industrial processes caused by unexpected failures of induction motors, preventive maintenance strategies are getting more popular since early diagnostics of incipient faults in induction motors are important to ensure safe operation and help to recognize and fix the problems with low costs and time. Motivating from the preventive maintenance approach, induction motors faults that frequently encountered in industry are created synthetically on test motors. In order to clarify the indicators of fault types definitely, certain faults are created synthetically on new test motors.

In this thesis, proposed classification tools are Bayesian originated classifiers: linear and quadratic discriminant classifiers, Fisher's linear discriminant based classifier, and Neural Network (NN) based classification algorithm self-organizing maps (SOM) and learning vector quantization (LVQ) techniques. These classifiers are utilized in fault classification of current, vibration and sound data obtained from various experiments realized. Classification results of different cases are given in and classification performances of different type of classifiers and selected filter types are also discussed. Current, vibration and acoustic data performances with same features are discussed to show the convenience of data type for classification.

During experiments, test motors are operated under different loading conditions in order to construct classification methods which provide reliable classification performances regardless of load. Besides, stator current data of test motors are acquired under the cases of both driven directly with AC line and driven with adjustable speed drive (ASD) experiments are realized. In the case of placing an ASD to test procedure, it is known that due to the pulse-width modulation (PWM) switching of the voltage source inverter, the motor current waveforms can be obstructed by the noise-like additive waveforms which conceal the fault

characteristics on stator current. Even in this challenging case, the proposed Wavelet Packet Decomposition (WPD) based feature extraction method showed great success for the classification of motor faults. The effect of filter type selection in WPD process is also critical since with increase of the level of decomposition, convolution of selected wavelet filter with data in a node to obtain decomposition coefficients may become meaningless if the selected filter size is almost equal or longer than the data length in a node. In order to see the effect of selected filter type in WPD, different wavelet types are tested during classification experiments. Besides, different classifiers are applied to the feature sets in order to obtain lower classification errors.

In addition to stator current, vibration and acoustic data based feature extraction techniques are used for fault classification. Novel feature extraction methods which use 2D representations of data signals are proposed. By 2D representation of the signal, classification with texture related features is possible if a priori knowledge of the classes to be recognized does exist. Appropriate texture based techniques can be applied for the classifications of the patterns caused by indicators like vibration and acoustic signals. Utilizing 2D discrete Wavelet Transformation to the grayscale image representations obtained from test data, the properties of the formed sub-images are used for feature indicators and give fairly good performances on vibration and acoustic based analysis. Texture based feature extraction methods found inefficient for current data since the nature of data is less random which may result in strict texture patterns in acquired grayscale images.

Unlike current and vibration based methods, there is very limited literature on fault diagnosis of induction motors which is based on acoustic analysis. Besides, some of these works analyze the acoustic data which are recorded in an echo-free silent environment, which seems impractical for the real life applications, especially in industrial processes. Instead of echo-free silent environment, acoustic data are collected from quite noisy laboratory environment which resembles a real industrial environment and this type of fault classification can be considered as another novelty about this thesis. Acoustic data are acquired in laboratory environment with ambient noise via five microphones surrounding the test rig. In order to classify different motor faults, cross-correlation coefficients between microphone channels

are used as attributes of the feature sets, which provide great increase on overall classification performance.

The local binary pattern (LBP) operator is an image operator which converts an image into an array or image having integer labels which describes small-scale appearance of the image. LBP is also utilized to the grayscale image representations of the acquired data signals. LBP is a highly discriminate operator which records the occurrences of various patterns in the neighborhood of each pixel in a histogram, and it is invariant to rotation changes of images. LBP histograms can be simply constructed from the images and the properties of the resulting histograms can be used for feature indicators. The last proposed method in this thesis is LBP histograms based classification. By using the fundamental statistical properties of the histogram and the autocorrelation of the histogram data with itself as feature vectors, classification performances of the different types of data are tested. Again as in other 2D representation methods, current data failed to classify but acoustic and vibration data provide quite enough success. Also when compared to other wavelet based feature extraction techniques proposed, LBP histogram methods require minimal computational cost.

To summarize, this thesis provides novel feature extraction techniques from current, vibration and acoustic data which are acquired in real industry-like laboratory environment. Quite well classification performances are reached by proper selection of the filtering method and classifier type. Besides, a remarkable benchmark database is constructed consisting of stator current, vibration and acoustic data acquired under many operating conditions. This database is expected to be used as medium for future works of fault diagnosis related to preventive maintenance strategies of the induction motors, which may be considered as a natural consequence of this thesis work.

REFERENCES

Acosta, G., Verucchi, C. and Gelso, E. (2006), "A current monitoring system for diagnosing electrical failures in induction motors," *Mechanical Systems and Signal Processing*, **20**(4), 953-965.

Akansu, A. N. and Haddad, R. A. (2001), "*Multiresolution signal decomposition: transforms, subbands, and wavelets*," Academic Press.

Akcay, H. and Germen, E. (2015), "Subspace-Based Identification of Acoustic Noise Spectra in Induction Motors," *IEEE Transactions on Energy Conversion*, **30**(1), 32-40.

Amar, M., Gondal, I. and Wilson, C. (2015), "Vibration spectrum imaging: A novel bearing fault classification approach," *IEEE Transactions on Industrial Electronics*, **62**(1), 494-502.

Arivazhagan, S. and Ganesan, L. (2003), "Texture classification using wavelet transform," *Pattern Recognition Letters*, **24**(9-10), 1513-1521.

Avci, E., Sengur, A. and Hanbay, D. (2009), "An optimum feature extraction method for texture classification," *Expert Systems with Applications*, **36**(3), 6036-6043.

Ayhan, B., Chow, M.-Y. and Song, M.-H. (2005), "Multiple signature processing-based fault detection schemes for broken rotor bar in induction motors," *IEEE Transactions on Energy Conversion*, **20**(2), 336-343.

Bellini, A., Filippetti, F., Tassoni, C. and Capolino, G.-A. (2008), "Advances in diagnostic techniques for induction machines," *IEEE Transactions On Industrial Electronics*, **12**(55), 4109-4126.

Benbouzid, M. (1999), "Bibliography on induction motors faults detection and diagnosis," *IEEE Transactions On Energy Conversion*, **14**(4), 1065-1074.

Benbouzid, M. E. H. and Kliman, G. B. (2003), "What stator current processing-based technique to use for induction motor rotor faults diagnosis?," *IEEE Transactions on Energy Conversion*, **18**(2), 238-244.

Benko, U., Petrovcic, J., Juricic, D., Tavcar, J., Rejec, J. and Stefanovska, A. (2004), "Fault diagnosis of a vacuum cleaner motor by means of sound analysis," *Journal of Sound and Vibration*, **276**(3-5), 781-806.

Chapman, S. (2005), "*Electric machinery fundamentals*," Tata McGraw-Hill Education.

Chong, U.-P. (2011), "Signal model-based fault detection and diagnosis for induction motors using features of vibration signal in two-dimension domain," *Strojniski Vestnik-Journal of Mechanical Engineering*, **57**(9), 655-666.

Dalvand, F., Keshavarzi, M., Kalantar, A. and Cheraghdar, A. (2015), "Detection of generalized-roughness bearing fault using statistical-time indices of instantaneous frequency of motor voltage space vector," *Proceedings of the Electrical Engineering (ICEE), 2015 23rd Iranian Conference on*, IEEE, 1516-1521.

Douglas, H., Pillay, P. and Ziarani, A. K. (2004), "A new algorithm for transient motor current signature analysis using wavelets," *IEEE Transactions on Industry Applications*, **40**(5), 1361-1368.

Duda, R. O., Hart, P. E. and Stork, D. G. (2012), "*Pattern classification*," John Wiley & Sons.

Ece, D. G. and Başaran, M. (2011), "Condition monitoring of speed controlled induction motors using wavelet packets and discriminant analysis," *Expert Systems with Applications: An International Journal*, **38**(7), 8079-8086.

Ece, D. G. and Gerek, O. (2006), "A Novel Feature Vector Consisting of AR-MA Model Parameters for Motor Fault Classification," *2006 IEEE 14th Signal Processing and Communications Applications*.

Ece, D. G. and Gerek, O. N. (2004), "Power quality event detection using joint 2-D-wavelet subspaces," *IEEE Transactions on Instrumentation and Measurement*, **53**(4), 1040-1046.

Eren, L. and Devaney, M. J. (2004), "Bearing damage detection via wavelet packet decomposition of the stator current," *IEEE Transactions on Instrumentation and Measurement*, **53**(2), 431-436.

Ergin, S., Uzuntas, A. and Gulmezoglu, M. B. (2012), "Detection of stator, bearing and rotor faults in induction motors," *Procedia Engineering*, **30**, 1103-1109.

Filippetti, F., Franceschini, G., Tassoni, C. and Vas, P. (1998), "AI techniques in induction machines diagnosis including the speed ripple effect," *IEEE Transactions on Industry Applications*, **34**(1), 98-108.

Finley, W. R., Hodowanec, M. M. and Holter, W. G. (1999), "An analytical approach to solving motor vibration problems," *Proceedings of the Petroleum and Chemical Industry Conference, 1999. Industry Applications Society 46th Annual*, IEEE, 217-232.

Fisher, R. A. (1936), "The use of multiple measurements in taxonomic problems," *Annals of eugenics*, **7**(2), 179-188.

Fitzgerald, A. E., Kingsley, C., Umans, S. D. and James, B. (1990), "*Electric machinery*," McGraw-Hill New York.

Gan, Z., Zhao, M.-B. and Chow, T. W. (2009), "Induction machine fault detection using clone selection programming," *Expert Systems with Applications*, **36**(4), 8000-8012.

Gerek, O. N. and Ece, D. G. (2004), "2-D analysis and compression of power-quality event data," *IEEE Transactions on Power Delivery*, **19**(2), 791-798.

Germen, E., Başaran, M. and Fidan, M. (2014), "Sound based induction motor fault diagnosis using Kohonen self-organizing map," *Mechanical Systems and Signal Processing*, **46**(1), 45-58.

Germen, E., Ünlü, Ü. and Kaya, A. (2010), "Effects of sound radiation direction in faulty hermetic compressors." *Proceedings of the International Compressor Engineering Conference*.

Gülmezoğlu, M. B. and Ergin, S. (2007), "An approach for bearing fault detection in electrical motors," *European Transactions on Electrical Power*, **17**(6), 628-641.

Günal, S., Ece, D. G. and Gerek, Ö. N. (2009), "Induction motor fault diagnosis via current analysis on time domain," *Proceedings of the Signal Processing and Communications Applications Conference, 2009. SIU 2009. IEEE 17th*, IEEE, 488-491.

Günal, S. and Gerek, Ö. N. (2009), "Induction machine condition monitoring using notch-filtered motor current," *Mechanical Systems and Signal Processing*, **23**(8), 2658-2670.

Henao, H., Capolino, G.-A., Fernandez-Cabanas, M., Filippetti, F., Bruzzese, C., Strangas, E., Pusca, R., Estima, J., Riera-Guasp, M. and Hedayati-Kia, S. (2014), "Trends in fault diagnosis for electrical machines: A review of diagnostic techniques," *Industrial Electronics Magazine, IEEE*, **8**(2), 31-42.

Immovilli, F., Bellini, A., Rubini, R. and Tassoni, C. (2010), "Diagnosis of bearing faults in induction machines by vibration or current signals: A critical comparison," *IEEE Transactions on Industry Applications*, **46**(4), 1350-1359.

Kaya, A., Germen, E., Ünlü, Ü. and Toprak, S. (2008), "Fault Classification in Hermetic Compressors Using Self-Organizing Map." *Proceedings of the International Compressor Engineering Conference.*

Kliman, G., Koegl, R., Stein, J., Endicott, R. and Madden, M. (1988), "Noninvasive detection of broken rotor bars in operating induction motors," *IEEE Transactions on Energy Conversion*, **3**(4), 873-879.

Knight, A. M. and Bertani, S. P. (2005), "Mechanical fault detection in a medium-sized induction motor using stator current monitoring," *IEEE Transactions on Energy Conversion*, **20**(4), 753-760.

Kohonen, T. (1990), "The Self-Orginizing Map," *Proceedings of the IEEE*, **78**(9), 1464-1480.

Kohonen, T. (1995), "*Learning vector quantization*," Springer.

Kuncheva, L. I. (2004), "*Combining pattern classifiers: methods and algorithms*," John Wiley & Sons.

Lee Rodgers, J. and Nicewander, W. A. (1988), "Thirteen ways to look at the correlation coefficient," *The American Statistician*, **42**(1), 59-66.

Loránd, S., Jenő, D., Biró, B. and Ágoston, K. (2004), "Rotor faults detection in squirrel-cage induction motors by current signature analysis."

Mäenpää, T. (2003), "*The Local binary pattern approach to texture analysis: Extenxions and applications*," Oulun yliopisto.

Nandi, S., Toliyat, H. A. and Li, X. D. (2005), "Condition monitoring and fault diagnosis of electrical motors - A review," *IEEE Transactions on Energy Conversion*, **20**(4), 719-729.

Ocak, H., Loparo, K. A. and Discenzo, F. M. (2007), "Online tracking of bearing wear using wavelet packet decomposition and probabilistic modeling: A method for bearing prognostics," *Journal of Sound and Vibration*, **302**(4), 951-961.

Ojala, T., Pietikäinen, M. and Harwood, D. (1996), "A comparative study of texture measures with classification based on featured distributions," *Pattern Recognition*, **29**(1), 51-59.

Penman, J., Sedding, H., Lloyd, B. and Fink, W. (1994), "Detection and location of interturn short circuits in the stator windings of operating motors," *IEEE Transactions on Energy Conversion*, **9**(4), 652-658.

Pietikäinen, M., Hadid, A., Zhao, G. and Ahonen, T. (2011), "Local binary patterns for still images," *Computer Vision Using Local Binary Patterns*, Springer**,** 13-47.

Rao, C. R. (1948), "The utilization of multiple measurements in problems of biological classification," *Journal of the Royal Statistical Society. Series B (Methodological)*, **10**(2), 159-203.

Samanta, B. and Al-Balushi, K. (2003), "Artificial neural network based fault diagnostics of rolling element bearings using time-domain features," *Mechanical Systems and Signal Processing*, **17**(2), 317-328.

Schoen, R. R., Lin, B. K., Habetler, T. G., Schlag, J. H. and Farag, S. (1995), "An unsupervised, on-line system for induction motor fault detection using stator current monitoring," *IEEE Transactions on Industry Applications*, **31**(6), 1280-1286.

Shahriar, M. R., Ahsan, T. and Chong, U. (2013), "Fault diagnosis of induction motors utilizing local binary pattern-based texture analysis," *EURASIP Journal on Image and Video Processing*, **2013**(1), 1-11.

Siddique, A., Yadava, G. and Singh, B. (2005), "A review of stator fault monitoring techniques of induction motors," *IEEE Transactions on Energy Conversion*, **20**(1), 106-114.

Tavner, P. (2008), "Review of condition monitoring of rotating electrical machines," *Electric Power Applications, IET*, **2**(4), 215-247.

Tavner, P. J. and Penman, J. (1987), "*Condition monitoring of electrical machines*," Research Studies Pre.

Teotrakool, K., Devaney, M. J. and Eren, L. (2009), "Adjustable-speed drive bearing-fault detection via wavelet packet decomposition," *IEEE Transactions on Instrumentation and Measurement*, **58**(8), 2747-2754.

Thomson, W. T. (2001), "On-line MCSA to diagnose shorted turns in low voltage stator windings of 3-phase induction motors prior to failure," *Proceedings of the Electric Machines and Drives Conference, 2001. IEMDC 2001. IEEE International*, IEEE, 891-898.

Thomson, W. T. and Fenger, M. (2001), "Current signature analysis to detect induction motor faults," *Industry Applications Magazine, IEEE*, **7**(4), 26-34.

Toliyat, H. A., Nandi, S., Choi, S. and Meshgin-Kelk, H. (2012), "*Electric machines: modeling, condition monitoring, and fault diagnosis*," CRC Press.

Trajin, B., Regnier, J. and Faucher, J. (2010), "Comparison between vibration and stator current analysis for the detection of bearing faults in asynchronous drives," *Electric Power Applications, IET*, **4**(2), 90-100.

Tuceryan, M. and Jain, A. K. (1993), "Texture analysis," *Handbook of pattern recognition and computer vision*, **2**, 207-248.

Van Der Heijden, F., Duin, R., De Ridder, D. and Tax, D. M. (2005), "*Classification, parameter estimation and state estimation: an engineering approach using MATLAB*," John Wiley & Sons.

Van Gool, L., Dewaele, P. and Oosterlinck, A. (1985), "Texture analysis anno 1983," *Computer vision, graphics, and image processing*, **29**(3), 336-357.

Welling, M. (2005), "Fisher linear discriminant analysis," *Department of Computer Science, University of Toronto*, **3**.

Widodo, A. and Yang, B.-S. (2008), "Wavelet support vector machine for induction machine fault diagnosis based on transient current signal," *Expert Systems with Applications*, **35**(1), 307-316.

Widodo, A., Yang, B.-S. and Han, T. (2007), "Combination of independent component analysis and support vector machines for intelligent faults

diagnosis of induction motors," *Expert Systems with Applications*, **32**(2), 299-312.

Williamson, S. and Mirzoian, K. (1985), "Analysis of cage induction motors with stator winding faults," *IEEE Transactions on Power Apparatus and Systems*, **7**(PAS-104), 1838-1842.

Yan, R. and Gao, R. X. (2006), "Hilbert–Huang transform-based vibration signal analysis for machine health monitoring," *IEEE Transactions on Instrumentation and Measurement*, **55**(6), 2320-2329.

Zhang, Z., Ren, Z. and Huang, W. (2003), "A novel detection method of motor broken rotor bars based on wavelet ridge," *IEEE Transactions on Energy Conversion*, **18**(3), 417-423.